AGU PUBLICATIONS

JGR

Journal of Geophysical Research: Oceans

RESEARCH ARTICLE

10.1002/2015JC011535

Key Points:
- The DIC maximum is a persistent feature of the Canada Basin halocline
- Conservative and nonconservative sources of DIC were investigated
- Upstream shelf sediment organic matter remineralization is the primary source of DIC

Correspondence to:
K. A. Brown,
kbrown@whoi.edu

Citation:
Brown, K. A., F. McLaughlin, P. D. Tortell, M. Yamamoto-Kawai, and R. Francois (2016), Sources of dissolved inorganic carbon to the Canada Basin halocline: A multitracer study, *J. Geophys. Res. Oceans*, *121*, 2918–2936, doi:10.1002/2015JC011535.

Received 6 DEC 2015
Accepted 28 MAR 2016
Accepted article online 31 MAR 2016
Published online 4 MAY 2016

Sources of dissolved inorganic carbon to the Canada Basin halocline: A multitracer study

Kristina A. Brown[1,2], Fiona McLaughlin[3], Philippe D. Tortell[1,4], Michiyo Yamamoto-Kawai[5], and Roger Francois[1]

[1]Department of Earth, Ocean and Atmospheric Sciences, University of British Columbia, Vancouver, British Columbia, Canada, [2]Now at Department of Marine Chemistry and Geochemistry, Woods Hole Oceanographic Institution, Woods Hole, Massachusetts, USA, [3]Fisheries and Oceans Canada, Institute of Ocean Sciences, Sidney, British Columbia, Canada, [4]Department of Botany, University of British Columbia, Vancouver, British Columbia, Canada, [5]Center for Advanced Science and Technology, Tokyo University of Marine Science and Technology, Tokyo, Japan

Abstract We examine the dissolved inorganic carbon maximum in the Canada Basin halocline using a suite of geochemical tracers to gain insight into the factors that contribute to the persistence of this feature. Hydrographic and geochemical samples were collected in the upper 500 m of the southwestern Canada Basin water column in the summer of 2008 and fall of 2009. These observations were used to identify conservative and nonconservative processes that contribute dissolved inorganic carbon to halocline source waters, including shelf sediment organic matter remineralization, air-sea gas exchange, and sea-ice brine export. Our results indicate that the remineralization of organic matter that occurs along the Bering and Chukchi Sea shelves is the overwhelming contributor of dissolved inorganic carbon to Pacific Winter Water that occupies the middle halocline in the southwestern Canada Basin. Nonconservative contributions from air-sea exchange and sea-ice brine are not significant. The broad salinity range associated with the DIC maximum, compared to the narrow salinity range of the nutrient maximum, is due to mixing between Pacific and Atlantic water and not abiotic addition of DIC.

1. Introduction

The Arctic Ocean is a hydrographically complex enclosed sea, with large-scale freshwater inputs from rivers and North Pacific inflow combined with oceanic heat and salt inputs from the North Atlantic. In contrast to the other three Arctic subbasins, where Pacific waters are mostly absent, the upper waters of the Canada Basin are composed of a vertically stacked, multihalocline complex maintained by waters from a variety of source regions. While surface water flows are controlled by the dominant atmospheric circulation [e.g., *Proshutinsky*, 2002; *McLaughlin et al*., 2011], lateral advection of shelf modified dense waters is the major process that contributes to the subsurface halocline [e.g., *Aagaard et al*., 1981; *Melling and Lewis*, 1982; *Aagaard and Carmack*, 1994]. The combination of high riverine input, the seasonal cycle of sea-ice formation and melt, and the inflow of Pacific water maintain the strong stratification and high nutrient content of the Canada Basin halocline [e.g., *Aagaard and Carmack*, 1989; *McLaughlin et al*., 2004, 2011].

Below the seasonally mixed surface layer, the Canada Basin halocline consists of three components: the upper, middle, and lower halocline [cf. *McLaughlin et al*., 2011, Figure 2a]. Inflowing water from the Pacific, via the Bering and Chukchi Sea shelves, dominates the upper and middle halocline of the Canada Basin. These high nutrient Pacific waters are modified by seasonal processes during transit across these shelves, including sea-ice formation/melting, biological productivity, sediment interaction [e.g., *Coachman et al*., 1975; *Shimada*, 2005; *Yamamoto-Kawai et al*., 2008], and intermittent mixing with inflowing East Siberian Sea water [e.g., *Anderson et al*., 2010]. Pacific Summer Water (PSW) transits the Chukchi Shelf in summer to supply the upper halocline and is characterized by a local temperature (T) maximum between salinity (S) = 31 and S = 32 [*Coachman and Barnes*, 1961; *Shimada et al*., 2001], as well as low-nutrient and high-oxygen concentrations associated with biological production in the Chukchi Sea [*McLaughlin et al*., 2004]. Pacific Winter Water (PWW) transits during winter to supply the middle halocline and is characterized by near-freezing T at S $\approx$ 33.1 [*Melling and Moore*, 1995; *Cooper et al*., 1997; *Shimada*, 2005]. The predominant features of PWW are the persistent and laterally extensive maxima in nutrients and dissolved inorganic

carbon (DIC) [e.g., *Moore et al*., 1983; *Jones and Anderson*, 1986; *Anderson et al*., 2010]. The strong stable stratification of the halocline complex isolates deeper layers from the surface, effectively sequestering this high-carbon, high-nutrient reservoir from the upper water column where it could otherwise contribute to increased primary production [e.g., *McLaughlin and Carmack*, 2010] or CO_2 efflux to the atmosphere [e.g., *Cai et al*., 2010]. While the nutrient and DIC maxima are thought to be at least partially derived from sedimentary organic matter (OM) remineralization, as PWW flows over the highly productive Bering and Chukchi Sea shelves in winter [e.g., *Aagaard et al*., 1981; *Jones and Anderson*, 1986; *Cooper et al*., 1997], contributions from other processes that could potentially alter DIC concentrations in halocline source waters have received limited attention until recently [e.g., *Bates*, 2006; *Bates et al*., 2011; *Cai et al*., 2014].

Conservative (dilution/concentration) and other nonconservative (air-sea gas exchange and sea-ice brine rejection) processes can also influence DIC concentrations in Pacific waters during their transit to the Canada Basin. For example, photosynthetic draw down of DIC in the highly productive Bering and Chukchi Seas in summer leaves surface waters of the continental shelf undersaturated with respect to CO_2 at the end of the growing season [e.g., *Murata and Takizawa*, 2003; *Bates et al*., 2005; *Kaltin and Anderson*, 2005]. These surface waters cool as autumn commences which increases CO_2 solubility and enhances their capacity to take up CO_2 from the atmosphere. The progressive cooling of CO_2 undersaturated waters allows the direct uptake of CO_2 via air-sea gas exchange as these Pacific waters transit the shelf in early winter, and in polynyas during winter, which increase their DIC content without a proportional change in nutrient concentrations. This solubility-driven CO_2 uptake could contribute to the shelf-basin carbon pump that transports CO_2 into the deep basin halocline as denser winter waters flow off shelf [e.g., *Bates*, 2006].

The formation of sea ice can also contribute DIC to Pacific waters in a nonconservative manner. Recent studies in polar coastal seas suggest that CO_2 is released into the underlying surface waters when sea ice forms [*Rysgaard et al*., 2007], resulting in enhanced DIC rejection relative to salinity. CO_2 is produced from the inorganic precipitation of carbonate mineral salts ($CaCO_3$) within the high-salinity brines of forming sea ice. Higher mobility of CO_2 within the brine channel network, relative to solid carbonate salts and brine, promotes the diffusion of CO_2 toward the interfaces of the forming ice (ice-water or ice-atmosphere), which increases dissolved CO_2 and DIC concentration in surface waters and leaves the solid $CaCO_3$ and alkalinity trapped within the ice [*Rysgaard et al*., 2007]. This sea-ice-driven rejection of CO_2 into surface waters could thus also contribute to the shelf-basin carbon pump if impacted surface waters are dense enough to sink and flow off-shelf [*Anderson et al*., 2004; *Rysgaard et al*., 2007; *Loose et al*., 2011]. Indeed, several studies have demonstrated a direct contribution of DIC to the water column associated with sea-ice formation [e.g., *Omar et al*., 2005; *Rysgaard et al*., 2007; *Miller et al*., 2011], suggesting that this "sea-ice-driven carbon pump" could be a significant source of DIC to the surface mixed layer in regions of intense sea-ice formation [*Rysgaard et al*., 2011]. If the sea-ice-driven rejection of CO_2 is important to winter water modification in the shelf seas, the sequestration of DIC within the Canada Basin halocline may be sensitive to changes in seasonal sea-ice formation along its shallow shelf margins. At present, no data sets exist to quantitatively examine the contribution of the sea-ice-driven carbon pump to the Canada Basin halocline.

Stable carbon isotopes of DIC (δ^{13}C-DIC) can provide a way to distinguish DIC contributions from different sources. Carbon isotope and nutrient tracers have been applied to distinguish air-sea gas exchange from biological DIC uptake/remineralization in several global ocean studies [e.g., *Broecker and Maier-Reimer*, 1992; *Lynch-Stieglitz et al*., 1995], in particular within the North Pacific and Southern Oceans, but these tracers have yet to be applied in the Arctic Ocean. Additionally, stable carbon isotope data could also be useful in tracing sea-ice-derived DIC, if the inorganic carbon added to surface waters via brine export carries a distinct isotopic signature compared to the seawater below [*Papadimitriou et al*., 2004].

Here we examine the DIC maximum in the Canada Basin halocline using a suite of geochemical tracers to gain insight into the factors that contribute to the persistence of this feature. We present nutrient, oxygen, DIC, and stable isotope (δ^{18}O-H_2O and δ^{13}C-DIC) data from the upper 500 m of the southwestern Canada Basin water column, collected in the summer of 2008 and fall of 2009, and use them to distinguish among the contributions of shelf sediment remineralization, air-sea gas exchange, and sea-ice brine export to the PWW layer DIC maximum.

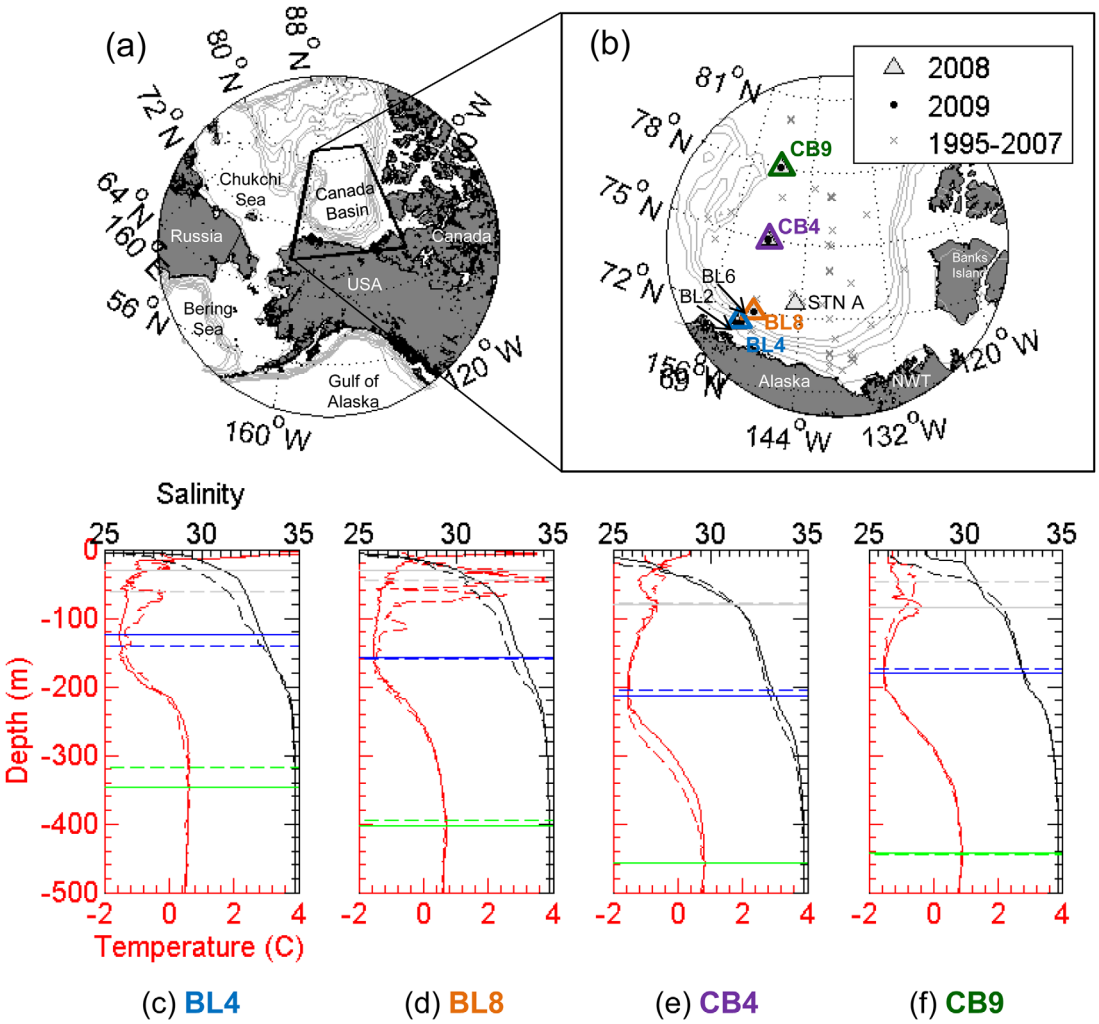

Figure 1. (a) Map of the study region in the Pacific-sector Arctic Ocean. Grey lines show bathymetry from 0 to 3000 m (500 m interval), and the black polygon indicates the location of stations occupied by the JOIS program from 1997 to 2009 (inset plot); (b) inset plot of the Canada Basin study region, grey lines show bathymetry from 0 to 2000 m depth (interval 250 m), with station locations illustrated as triangles (2008) and circles (2009); (c–f) temperature (red) and salinity (black) profiles in the upper 500 m of the water column profiles from four representative stations during the 2008 (solid lines) and 2009 (dashed lines) cruises. Grey, blue, and green horizontal lines refer to the depths of the subsurface temperature maximum (Pacific Summer Water), subsurface temperature minimum (Pacific Winter Water), and the Atlantic layer T-maximum, in 2008 (solid lines) and 2009 (dashed lines), respectively.

2. Sample Collection and Analytical Methods

2.1. Sampling and Analyses of Geochemical Parameters

Hydrographic observations and geochemical samples presented in this study were collected aboard the *CCGS Louis S St-Laurent* as part of the Canada-U.S. Joint Ocean Ice System Study (JOIS) and the International Polar Year Canada's Three Oceans (IPY-C3O) program. Data were collected at a subset of stations along the program transect from the shallow shelf near Barrow Alaska toward the north-east into the deep central Canada Basin (Figures 1a and 1b), in the summer of 2008 (17 July to 21 August) and fall of 2009 (17 September to 15 October). These data were compared with historical hydrographic and geochemical data (1997–2007) from summer cruises throughout the Canada Basin which are available through the Canadian Data Report of Hydrography and Ocean Sciences series and the Woods Hole Oceanographic Institution Beaufort Gyre Observational System (http://www.whoi.edu/page.do?pid=66521).

Water column samples were collected from 10 L Niskin bottles mounted on an ice-strengthened CTD rosette system, following the methods outlined in *McLaughlin et al.* [2012]. Analytical precision for each geochemical parameter measured in this study is listed in Table 1 and presented as the pooled standard deviation of all replicate measurements (*SDp*). *SDp* is calculated for a series of duplicate sample measurements (x_1 and x_2) carried out under similar conditions and is determined as $SDp=[\sum (xi_1-xi_2)^2/2k]^{1/2}$, where k is

Table 1. Pooled Standard Deviation (*SDp*) of Duplicate Geochemical Analyses

		2008		2009	
Parameter	Units	*SDp*	k	*SDp*	k
S		0.002	156	0.007	134
NO_3	mmol m^{-3}	0.08	247	0.07	191
NH_4^+	mmol m^{-3}	0.04	163	0.02	120
PO_4	mmol m^{-3}	0.01	242	0.01	206
Oxygen	mmol m^{-3}	1.340[a]	181	0.313[a]	195
$\delta^{18}O$	‰ V-SMOW	0.04	13	0.03	20
DIC	μmol kg^{-1}	3.65	35	3.65	35
TAlk	μmol kg^{-1}	3.49	11	3.49	11
δ^{13}C-DIC	‰ V-PDB	0.01[b]	217[b]	0.01[b]	217[b]

[a]Oxygen *SDp* was determined as mL/L and converted to mmol m^{-3} by multiplying by 44.661.
[b]2008 and 2009 analyzed as a single set.

the number of duplicate pairs analyzed [*IUPAC*, 1997]. It is assumed that measurements carried out under similar conditions are of the same precision, although their means may differ, and as such, *SDp* is a better estimate of the underlying standard deviation of the analyses than individual calculated standard deviations of k measurements [*IUPAC*, 1997].

DIC was measured coulometrically following *Dickson et al.* [2007] using either a VINDTA 3D or SOMMA-I system at Fisheries and Oceans Canada's Institute of Ocean Sciences. Total Alkalinity (TAlk) was determined using an open-cell continuous titration with an automated Dosimat 665 titrator (Metrohm) and Red Rod pH combination electrode (Radiometer Analytical). Endpoint detection was determined using a modified version of *Dickson et al.*'s [2007] LabView computer program. Both DIC and TAlk were calibrated against certified reference materials provided by Andrew Dickson (Batch 88, Scripps Institute of Oceanography). Carbon isotope (δ^{13}C-DIC) samples were analyzed at GEOTOP Stable Isotope Laboratory (University du Quebec à Montréal) using a Micromass Isoprime continuous flow isotope ratio mass spectrometer equipped with a MultiFlow (Isoprime) automated injection system. Carbon isotopic values are reported in per mil (‰) with respect to VPDB referenced to the NBS-19 and LSVEC scales (standard error $\pm$ 0.1‰). All δ^{13}C-DIC values reported in this study are based on duplicate analyses. Oxygen isotope ($\delta^{18}O$-H_2O) samples were analyzed following *Epstein and Mayeda* [1953] at Oregon State University's COAS Stable Isotope Lab using a Thermo Finnigan DeltaPlus XL isotope ratio mass spectrometer. Oxygen isotopic values are reported in per mil (‰) with respect to Vienna Standard Mean Ocean Water (V-SMOW) (standard error $\pm$ 0.05‰). Dissolved oxygen, salinity, nitrate (measured as nitrate + nitrite, herein referred to as NO_3), orthophosphate (PO_4), and ammonium (NH_4^+) samples were analyzed on board the *CCGS Louis S St-Laurent* in both years as described in *McLaughlin et al.* [2012]. Dissolved inorganic nitrogen (DIN) was determined from measured nutrient values ($DIN = NO_3 + NH_4^+$) and has an associated error of 0.09 and 0.07 mmol m^{-3} for 2008 and 2009, respectively. These error terms are derived by combining the analytical precision for NO_3 and NH_4^+ analyses (Table 1).

3. Calculations

3.1. Freshwater Components

Freshwater components of the water column were quantified from measured $\delta^{18}O$-H_2O (herein, $\delta^{18}O$), S, and nutrients (DIN and PO_4) as in *Yamamoto-Kawai et al.* [2008], using the following mass balance and N:P relationships (equations (1–8)). We characterized Canada Basin waters sampled in this study as a mixture of Arctic meteoric water (MW, which includes both river inflow and precipitation), sea-ice melt (SIM) or formation (-SIM), and a saline end-member (SE) [after *Östlund and Hut*, 1984]:

$$f_{SIM} + f_{MW} + f_{SE} = 1 \quad (1)$$

$$f_{SIM}S_{SIM} + f_{MW}S_{MW} + f_{SE}S_{SE} = S_{OBS} \quad (2)$$

$$f_{SIM}\delta^{18}O_{SIM} + f_{MW}\delta^{18}O_{MW} + f_{SE}\delta^{18}O_{SE} = \delta^{18}O_{OBS} \quad (3)$$

where subscripts SIM, MW, and SE refer to end-member composition (S and $\delta^{18}O$) as in Table 2, *f* refers to the fractional contribution of each component, and the subscript OBS refers to measured quantities. Following *Östlund and Hut* [1984], f_{SIM} becomes negative when brine is added to surface waters during sea-ice formation. Following *Yamamoto-Kawai et al.* [2008] and *Jones et al.* [1998], SE for Canada Basin waters with $S \leq 33$ is Pacific water (PW). For waters with $S > 33$, SE is a mixture of both Atlantic water (ATW) and PW, the proportions of which are determined using their nutrient composition. Briefly, the following N:P relationships have been derived for either ATW or PW, based on linear regressions:

$$DIN^{ATW} = 17.499 \times PO_4{}^{ATW} - 3.072 \quad (\text{for } S > 33 \text{ waters}, \ r^2 = 0.97) \tag{4}$$

$$DIN^{PW} = 13.957 \times PO_4{}^{PW} - 11.306 \quad (\text{for } S \leq 33 \text{ waters}, \ r^2 = 0.98) \tag{5}$$

and here we use DIN to account for the effects of nitrification on the N:P relationship of Pacific waters entering the Canada Basin (see *Yamamoto-Kawai et al*. [2008] for discussion). As there is no ammonium measurable in ATW in the Canada Basin, DIN $\approx NO_3$ in equation (4). For each measured DIN value in our data set, two phosphate values are computed, one based on the Pacific water line (P_{PW}; equation (5)), and one based on the Atlantic water line (P_{ATW}; equation (4)). The ratio of PW to ATW (R_{PW}) in each $S > 33$ sample is then determined from the observed phosphate concentration (P_{OBS}) and the calculated phosphate (P_{PW}, P_{ATW}) according to the ratio R_{PW} (equation (6); following *Yamamoto-Kawai et al*. [2008]):

$$R_{PW} = \frac{(P_{OBS} - P_{ATW})}{(P_{PW} - P_{ATW})} \tag{6}$$

Therefore, for $S > 33$ waters in the Canada Basin, S_{SE} and $\delta^{18}O_{SE}$ from equations (1–3) are determined as follows:

$$S_{SE} = S_{PW} \times R_{PW} + S_{ATW} \times (1 - R_{PW}) \tag{7}$$

$$\delta^{18}O_{SE} = \delta^{18}O_{PW} \times R_{PW} + \delta^{18}O_{ATW} \times (1 - R_{PW}) \tag{8}$$

Here we use end-member values following *Yamamoto-Kawai et al*. [2008] and given in Table 2. The PW end-member values are determined from mean near-bottom (~50 m) water properties in Bering Strait. SIM is derived from sea ice sampled within the Canada Basin and MW is obtained from Arctic river properties described by *Cooper et al*. [2008]. The ATW end-member values are obtained from the Eurasian Basin, upstream of the Canada Basin, as described by *Yamamoto-Kawai et al*. [2005]. The overall uncertainty in the calculation of freshwater fractions (f_{SIM} and f_{MW}) using our data set is ± 0.02, and results primarily from uncertainty in $\delta^{18}O$ analyses (Table 1). Seasonal variability in Bering Sea throughflow S (31.9–33) and $\delta^{18}O$ (-1.2 to $-0.5‰$) further influence f_{SIM} and f_{MW} calculations by ± 0.02 or less (as reported in *Yamamoto-Kawai et al*. [2009]). The potential error in the calculation of R_{PW} was determined to be < 0.14 when phosphate concentrations were between 1.5–2.3 and 0.6–1.1 μmol kg^{-1} for PW and ATW, respectively (see discussion in *Yamamoto-Kawai et al*. [2008]). For any samples with $S > 33$ but no accompanying nutrient data (31% of 2008 samples), R_{PW} was determined based on a regression of R_{PW} against salinity: $R_{PW} = -0.524 \times$ Salinity $+ 18.283$ ($r^2 = 0.979$), plotted from the remaining 2008 and 2009 data set ($n = 71$). Values of R_{PW} calculated with this regression have an estimated additional uncertainty of ± 0.06.

3.2. Salinity-Normalized DIC and PO_4

To correct for the influences of seawater concentration and dilution that change DIC and PO_4 proportionally with salinity, we normalized measured DIC and PO_4 values to $S = 35$ (equation (9)). For samples with a measureable meteoric water component ($f_{MW} > 0.02$), DIC data were normalized to account for the addition of DIC by freshwater input following *Friis et al*. [2003] (equation (10)).

$$DIC_{norm} = \frac{DIC_{obs}}{S_{obs}} \times S_{35} \tag{9}$$

$$DIC_{norm} = \frac{(DIC_{obs} - DIC_{S=0})}{S_{obs}} \times S_{35} + DIC_{S=0} \tag{10}$$

Here DIC_{obs} refers to the observed DIC value and $DIC_{s=0}$ to the riverine and sea-ice melt DIC contribution. We chose a salinity of 35 to remove the influence of mixing between source water saline end-members (PW versus ATW) and extrapolated the DIC versus S plot over the sampled interval of $S = 25$ to 33.1 to determine the $DIC_{S=0}$ value of 1013 μmol kg^{-1} (note: this was carried out only for samples with significant MW component). Although the sea-ice melt contribution of DIC to

Table 2. Salinity and $\delta^{18}O$ End-Member Values Used to Determine Water Mass Composition [After *Yamamoto-Kawai et al*., 2009]

	Atlantic Water (ATW)	Pacific Water (PW)	Sea Ice Melt (SIM)	Meteoric Water (MW)
S	34.87 ± 0.03	32.5 ± 0.02	4 ± 1	0
$\delta^{18}O$ (‰)	0.24 ± 0.05	-0.8 ± 0.1	-2 ± 1.0	-20 ± 2

surface waters is not zero [e.g., *Rysgaard et al*., 2007], our regression to $DIC_{S=0}$ will include the influence of both river input and sea-ice melt and thus we do not apply any further correction to equation (10). Our $DIC_{S=0}$ value is consistent with previous estimates of average freshwater DIC contributions from the Yukon River, a major source of terrestrial DIC to the Chukchi and Bering Seas [*Cai et al*., 2014], which range from ≈690 to 1629 μmol L^{-1} [*Kaltin and Anderson*, 2005; *Guo et al*., 2012] (PARTNERS data http://www.arcticgreatrivers.org/data.html). Normalized values of DIC and PO_4 were calculated only if there was enough information to determine the f_{MW} for the sample.

We chose not to correct PO_4 for riverine or sea-ice melt contributions because the PO_4 versus S plot has a negative intercept. The majority of river-derived nutrients are likely quickly depleted in the coastal estuary due to high rates of primary production during the spring and summer when inputs are highest.

3.3. AOU

We determined Apparent Oxygen Utilization (AOU) in halocline waters following *Sarmiento and Gruber* [2006], as in equation (11):

$$AOU = (O_{2\,sat} - O_{2\,meas}) \tag{11}$$

where $O_{2\ sat}$ and $O_{2\ meas}$ are the calculated and measured saturation concentrations, respectively. O_2 saturation values were calculated using the T-dependent and S-dependent solubility function of *Weiss* [1970].

3.4. Nitrate Deficit, N*

Effects of denitrification on the nitrate:phosphate ratio of OM remineralization products can be determined by calculating N* (equation (12), following *Granger et al*. [2013]), a conservative tracer whose distribution in the oceans is impacted only by denitrification, nitrification, and water mass transport [*Gruber and Sarmiento*, 1997].

$$N^* = (DIN - 16{\times}PO_4 + 2.9)\ \mathrm{mmol\,m^3} \tag{12}$$

3.5. DIC Disequilibrium in Pacific Winter Water

Following *Yamamoto-Kawai et al*. [2011] (equation (13)), the DIC disequilibrium (DIC_{diseq}) within PWW was determined as the observed DIC concentration of the sample (DIC_{obs}) minus the expected DIC concentration of the sample in equilibrium with the atmosphere (DIC_{eq}, @ measured S, T, TAlk, and P = 1 atm).

$$DIC_{diseq} = DIC_{obs} - DIC_{eq} \tag{13}$$

Measured TAlk, atmospheric pCO_2, S, and T were used to calculate DIC_{eq} using the MS Excel version of CO2Sys (co2sys_xls_program) [*Pierrot et al*., 2006], with equilibrium constants K_1 and K_2 defined by *Mehrbach et al*. [1973] and refit by *Dickson and Millero* [1987], and the dissociation constants for $KHSO_4$ determined by *Dickson* [1990]. We use the mean age of halocline PWW as 12 ± 5 years [*Anderson et al*., 2010] to determine the average atmospheric pCO_2 when PWW was last at the surface and, using annual average atmospheric pCO_2 values from Barrow Alaska provided by CDIAC (http://cdiac.ornl.gov/ftp/trends/co2/barr-sio.co2) for 1996 and 1997, we obtain an average pCO_2 value of 365 ppmv.

4. Results

The seasonal difference in sample collection in 2008 (late summer) and 2009 (fall after the onset of freezing) translated into widely different hydrographic and biogeochemical properties in the surface mixed layer [*Brown et al*., 2014]. In contrast, and as shown below, the geochemical features of the halocline are seasonally independent and representative of "averaged" properties, i.e., small-scale gradients are mixed away as Pacific waters flow off-shelf and contribute to the interior basin halocline [e.g., *Newton et al*., 2013].

4.1. General Hydrographic Profiles in the South-Western Canada Basin 2008 and 2009

The hydrographic and geochemical parameters from all the stations sampled during this study (2008 and 2009) are discussed below (and listed in Tables 3 and 4). Figures 1c–1f depict representative hydrographic profiles in the upper 500 m of the water column at two of the slope (BL4 ≈ 900 m and BL8 ≈ 3000 m; Figure 1b) and two of the deep basin (CB4 ≈ 3900 m and CB9 ≈ 3900 m; Figure 1b) stations.

Table 3. Hydrographic and Geochemical Properties of the Nutrient Maximum at Each Station (2008 and 2009)

Year	Station[a]	Latitude (°N)	CTD Pres (dbar)	CTD Temp (ITS-90 C)	CTD Salinity (PSS-78)	DIN (mmol m^{-3})	PO_4[b] (mmol m^{-3})	DIC (μmol kg^{-1})	δ^{13}C-DIC (‰)	f_{MW}[c]	f_{SIM}[c]	AOU (mmol m^{-3})	DICdiseq (μmol kg^{-1})	N* (mmol m^{-3})
2008	BL-2	71.396	126.9	−1.53	33.05	14.8	1.89	n.d.	0.60	0.045	−0.072	80.31	n.d.	−12.50
2008	CB-4	74.993	183.4	−1.55	32.89	14.4	1.82	n.d.	n.d.	n.d.	n.d.	80.55	n.d.	−11.80
2008	CB-9	78.003	207.1	−1.38	33.44	13.2	1.75	2227.47	n.d.	0.043	−0.071	86.24	62.35	−11.94
2008	Stn-A	72.601	181.2	−1.53	32.90	14.8	1.85	2206.89	0.60	0.044	−0.065	86.90	52.22	−11.90
2008 Average			174.7	−1.49	33.07	14.3	1.83	2217.18	0.60	0.044	−0.070	83.50	57.29	−12.03
2009	BL-2	71.396	103.5	−1.36	33.13	15.2	1.84	2210.78	n.d.	0.040	−0.058	95.21	56.78	−11.29
2009	BL-4	71.493	137.1	−1.41	33.02	15.1	1.82	2214.19	0.39	0.041	−0.059	88.40	51.10	−11.03
2009	BL-6	71.658	159.3	−1.47	32.96	15.1	1.84	2217.68	0.36	0.036	−0.059	91.99	45.59	−11.39
2009	BL-8	71.953	165.2	−1.50	32.95	15.7	1.87	2212.75	0.19	0.034	−0.056	94.74	47.16	−11.41
2009	CB-4	75.001	219.4	−1.53	33.11	14.9	1.81	2220.23	0.40	0.045	−0.065	84.81	57.57	−11.10
2009	CB-9	78.019	187.4	−1.50	33.16	15.5	1.85	2223.58	*0.31*	0.042	−0.063	90.12	54.92	−11.18
2009 Average			162.0	−1.46	33.05	15.3	1.84	2216.54	0.33	0.040	−0.060	90.88	52.19	−11.23

[a]The following stations had no nutrient data reported: BL4, BL6, BL8 (2008), and Stn-A (2009).
[b]Maximum PO_4 concentration measured in the profile at each station.
[c]f_{MW} and f_{SIM} refer to the fraction of meteoric water and fraction of sea ice melt water respectively, as described in the text.

The seasonal mixed layer in the Canada Basin occupied the upper ~25 m of the water column and was highly variable between the 2 years (Figures 1c–1f) [*Brown et al*., 2014]. Below this seasonal feature, the PSW layer of the upper halocline was found at an averaged depth of 90 m across all stations sampled. This water mass, characterized by a maximum in subsurface T, was found at S = 30.0–31.6 in 2008 and 2009 (light grey horizontal lines, Figures 1c–1f). For the subsequent discussion, we define the S of the PSW layer as S = 30.9 ± 0.6 based on the S of the subsurface T-maximum from our CTD profiles. The middle halocline PWW layer, characterized by a minimum in subsurface T, was observed at a depth of 120–220 m and a S range of 32.5–33.4 (blue horizontal lines, Figures 1c–1f) and, as described above, the S of the PWW layer was defined as S = 33.0 ± 0.2, the average S of the T-minimum. Compared to the shelf stations, the PWW layer was found deeper in the basin due to Ekman convergence and the accumulation of freshwater within the Beaufort Gyre [e.g., *Proshutinsky*, 2002; *McLaughlin and Carmack*, 2010]. Below the middle halocline, both T and S increased in the transition to ATW. We identify the core of the Fram Strait Branch of ATW by the deep T-maximum value in each CTD depth profile [after *McLaughlin et al*., 2004] which was observed at S = 34.81 ± 0.02 and a depth of ≈450 m at basin stations, shoaling to ≈330 m at the slope stations (green horizontal lines, Figures 1c–1f).

4.2. Geochemical Properties of the Water Column

Phosphate concentrations were low at the surface and gradually increased with depth through the PSW layer to reach a maximum in the PWW layer (Figure 2a). The PO_4 maximum at each station was determined from a depth profile of PO_4 concentration and was associated with the core of the PWW layer (T-minimum) in both years (Table 3). The nutrient maximum at each station in the full data set (1995–2009) showed little variability (PO_4 = 1.88 ± 0.09 mmol m^{-3}; n = 112), and was similarly associated with the PWW layer (S = 32.97 ± 0.26).

Table 4. Hydrographic and Geochemical Properties of the DIC Maximum at Each Station (2008 and 2009)

Year	Station[a]	Latitude (°N)	CTD Pres (dbar)	CTD Temp (ITS-90 C)	CTD Salinity (PSS-78)	DIN (mmol m^{-3})	PO_4 (mmol m^{-3})	DIC[b] (μmol kg^{-1})	δ^{13}C-DIC (‰)	f_{MW}[c]	f_{SIM}[c]	AOU (mmol m^{-3})	DICdiseq (μmol kg^{-1})	N* (mmol m^{-3})
2008	CB-4	75.021	227.0	−1.39	33.52	n.d.	n.d.	2239.38	n.d.	0.043	−0.061	82.96	64.36	n.d.
2008	CB-9	78.003	210.8	−1.29	33.58	14.7	1.70	2232.46	n.d.	n.d.	n.d.	92.92	58.95	−9.63
2008	Stn-A	72.601	222.8	−1.37	33.54	15.0	1.69	2222.97	0.54	0.034	−0.057	95.05	60.92	−9.12
2008 Average			220.2	−1.35	33.55	14.8	1.69	2231.60	0.54	0.039	−0.059	90.31	61.41	−9.38
2009	BL-2	71.396	140.9	−0.98	33.89	14.2	1.45	2212.34	0.60	0.025	−0.040	93.42	42.42	−6.16
2009	BL-4	71.493	158.2	−1.33	33.55	15.0	1.67	2221.49	0.29	0.038	−0.058	101.96	49.11	−8.82
2009	BL-6	71.658	172.1	−1.45	33.20	15.3	1.81	2227.84	0.44	0.044	−0.065	92.78	25.74	−10.68
2009	BL-8	71.953	179.6	−1.35	33.20	15.7	1.82	2215.76	0.30	0.038	−0.057	91.08	40.72	−10.55
2009	CB-4	75.001	248.3	−1.47	33.48	14.6	1.68	2228.22	n.d.	0.044	−0.067	84.07	52.96	−9.34
2009	CB-9	78.019	198.2	−1.41	33.37	15.1	1.76	2226.13	0.31	*0.018*	*−0.028*	91.99	78.75	−10.04
2009 Average			182.9	−1.33	33.45	15.0	1.70	2221.96	0.39	0.034	−0.053	92.55	48.28	−9.27

[a]The following stations had no DIC data reported: BL2, BL4, BL6, BL8 (2008), and Stn-A (2009).
[b]Maximum DIC concentration measured in the profile at each station.
[c]f_{MW} and f_{SIM} refer to the fraction of meteoric water and fraction of sea ice melt water respectively, as described in the text.

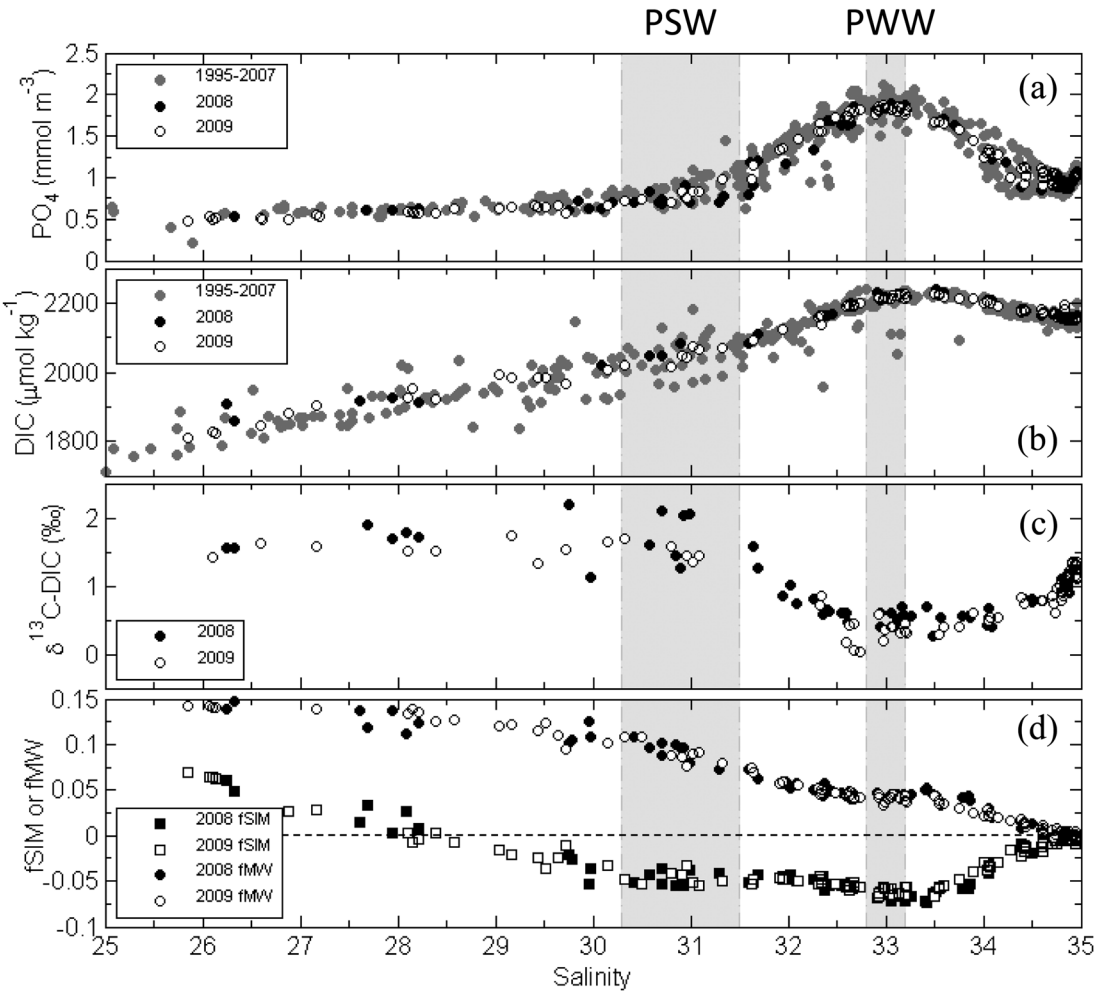

Figure 2. Tracer concentrations from the southwestern Canada Basin, collected in 2008 (black filled symbols), 2009 (white filled symbols), and from 1997 to 2007 (grey filled circles), plotted verses salinity. Historical data (1997–2007) are from station locations marked with crosses in Figure 1b. Shaded regions indicate average salinity of Pacific Summer Water (S = 30.9 ± 0.6) and Pacific Winter Water (S = 33.0 ± 0.2), and the black horizontal line in Figure 2d indicates zero.

This near-constant value and salinity-dependent distribution of the PO_4 maximum illustrates the interannual independence of the PWW layer.

Similarly, DIC concentrations were lowest in the low-S surface waters and increased toward the maximum values within the middle halocline (Figure 2b). As with the nutrient maximum, the DIC maximum at each station was determined from a profile of DIC concentration with depth (Table 4). The DIC maximum measured during this study (2225 ± 8 μmol kg^{-1}) was within that observed in the historical data set (2215 ± 21 μmol kg^{-1}; 1997–2007) and was invariably associated with the PWW layer. However, the DIC maxima from the combined data sets (our measurements plus archive data) occurred over a broader salinity range (cf. Table 4 and 1997–2007: S = 33.42 ± 0.54, n = 51) extending toward higher salinity than the nutrient maximum at almost every station sampled (Figure 3).

The stable isotopic composition of DIC (δ^{13}C-DIC) covered a wide range from +0.26 to +2.19‰ and +0.03 to +1.73‰ in 2008 and 2009, respectively (Figure 2c). The distribution of δ^{13}C-DIC nearly inversely mirrored that of DIC and PO_4. Isotopically heavy values were observed in low-salinity, low-nutrient surface waters, and in the ATW layer (S ≈ 34.8; Figure 2c), with a strong minimum present in the nutrient-rich halocline between S ≈ 32.59 and 34.04.

An increasingly negative f_{SIM}, indicative of sea-ice formation and the rejection of brine, started at S ≈ 28 to reach a maximum at S = 33.42 within the PWW layer (Figure 2d). Below PWW, the signal of sea-ice

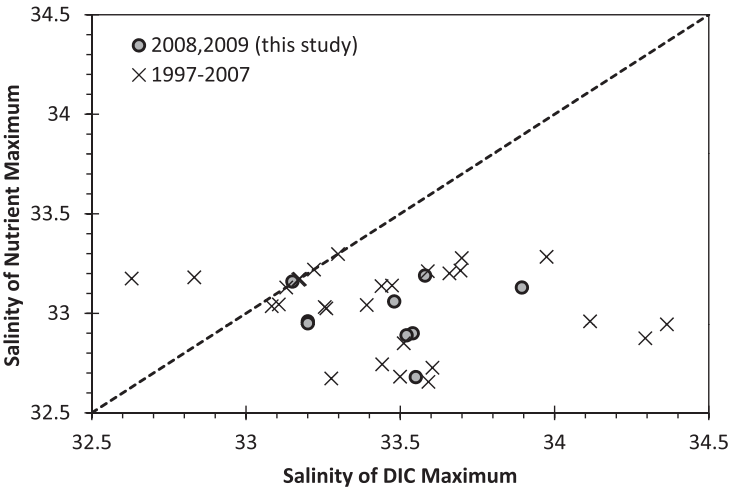

Figure 3. Comparison of the measured salinity associated with the maximum DIC concentration in each station profile plotted against the measured salinity associated with the maximum nutrient (PO_4) concentration. Data from this study (2008 and 2009) illustrated by filled circles and historical data from the JOIS cruises (1995–2007) indicated by crosses. The dashed line is a 1:1 line, values falling on this line indicate the salinity of both maxima are identical, in other words, DIC and PO_4 maximum from that profile were sampled from the same niskin bottle.

formation became eroded (less negative) with increased S due to mixing with $f_{SIM} \approx 0$ in the ATW layer. The presence of sea-ice melt water ($+f_{SIM}$) was observed only in waters with salinity less than 28.

5. Discussion

Samples collected from the southwestern Canada Basin in 2008 and 2009, and throughout the basin from 1995 to 2007, illustrate the persistence, and invariance on decadal time scales, of a DIC maximum associated with the PWW layer (middle halocline), a feature also observed in other studies [e.g., *Jones and Anderson*, 1986; *Anderson et al*., 1988, 2010; *Bates et al*., 2005]. The averaged maximum DIC concentration at each station exhibited a relatively narrow range (2225 $\pm$ 8 μmol kg^{-1}), and was similar between years (2008 and 2009) and seasons (summer and fall; Table 4). Unlike the nutrient maximum, which was confined to an S range coincident with the subsurface T-minimum (PWW layer), the DIC maximum spread over a broader S range. Previous studies [*Anderson et al*., 1990; *McLaughlin et al*., 2004; *Woodgate et al*., 2005; *Cai et al*., 2014] have also noted that the DIC maximum spreads over a broader S range than the nutrient maximum.

5.1. Contributors of DIC to the Canada Basin Middle Halocline (PWW)

Winter shelf waters, the source of PWW, can have their DIC content altered by both conservative and nonconservative processes. Conservative processes influencing DIC include water mass mixing, freshwater dilution (river water), and brine drainage during sea-ice formation, whereas nonconservative processes include air-sea exchange, sea-ice formation, and the formation/decay of OM. Although sea-ice formation and brine rejection can influence DIC both conservatively (with respect to S) and nonconservatively [*Rysgaard et al*., 2007], conservative changes of DIC resulting from sea-ice formation can be easily evaluated by normalizing measured DIC concentrations to a reference salinity (section 3.2; Figure 4a). Maximum values of S-normalized DIC (DIC_{norm}) at each station were indeed more closely associated with the S of the nutrient maximum (Figure 4a), however they still extended across a similar S range as the non-normalized values (cf. Figures 2b and 4a). This indicates that while sea-ice brine injection plays some role, the conservative concentration of DIC alone cannot account for the DIC increase between PSW and PWW. This further suggests that nonconservative sources are important in supplying DIC to the Canada Basin halocline.

Of the nonconservative processes, air-sea gas exchange and brine rejection can be distinguished from the formation and decay of OM when changes in DIC occur independently of nutrients and AOU. Sea-ice formation along the shallow shelves may result in a nonconservative addition of DIC to the water column if CO_2 and $CaCO_3$ are separated within the brine network and CO_2 is able to diffuse into surface waters under the newly forming ice [e.g., *Anderson et al*., 2004; *Rysgaard et al*., 2007]. As well, air-sea exchange could add DIC

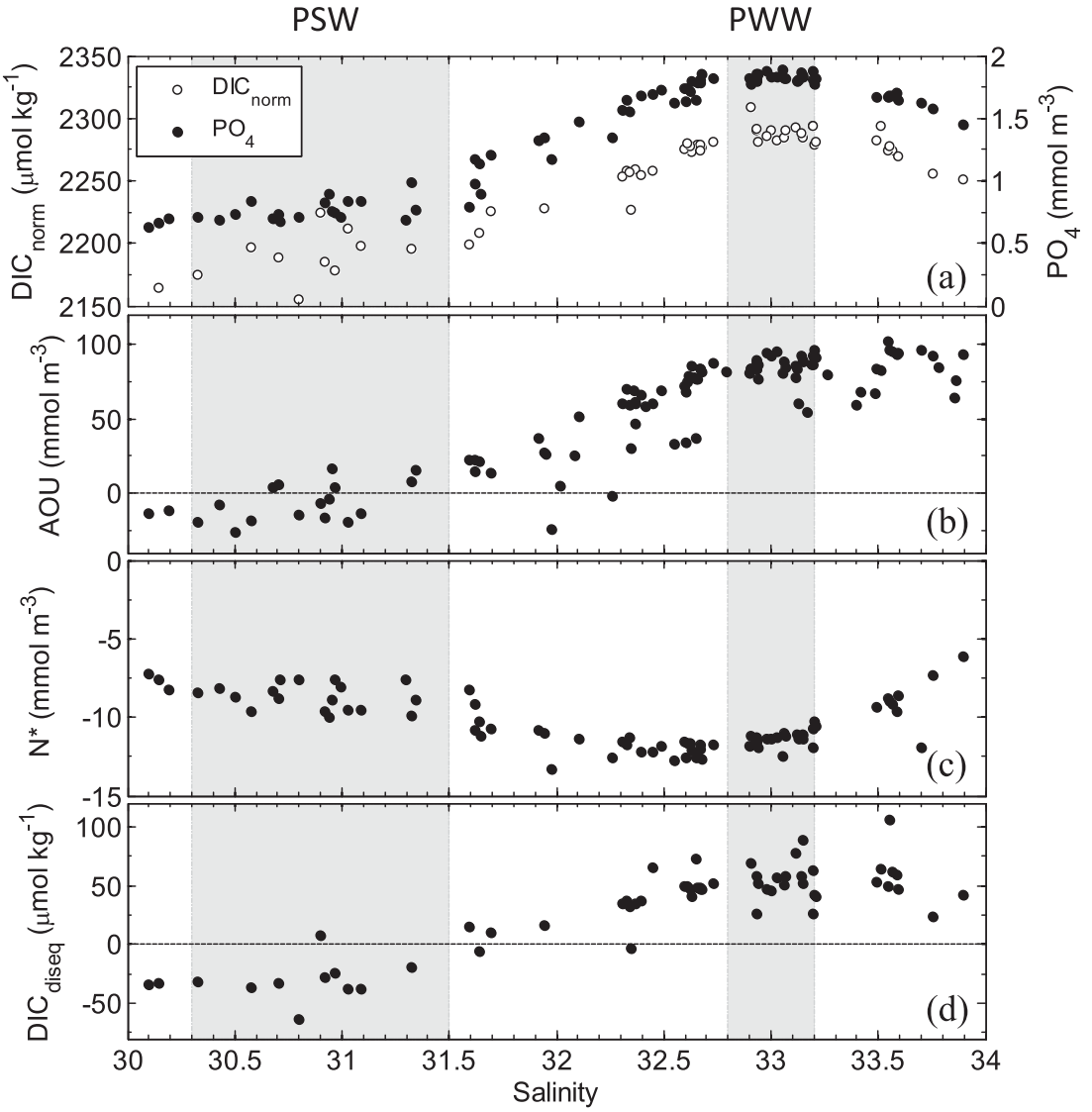

Figure 4. Tracer concentrations from the south-western Canada Basin halocline from both years (2008 and 2009) plotted verses salinity. Shaded regions indicate average salinity of PSW (S = 30.9 ± 0.6) and PWW (S = 33.0 ± 0.2), and the dashed horizontal lines in Figures 4b and 4d indicate zero.

to PWW during cooling in early winter. These two processes can potentially be distinguished from the formation and decay of OM by their effect on δ^{13}C-DIC. We now investigate the influence of nonconservative processes that affect both DIC and nutrient concentrations within PWW and then turn to an investigation of nonconservative processes that act on DIC concentrations alone (section 5.3).

5.2. Processes That Change Both DIC and Nutrient Inventories

Remineralization of OM within the Arctic Ocean, either along the shallow shelf seas or within the water column, has been cited as a major contributor to the high-nutrient and DIC concentrations within the Canada Basin middle halocline [e.g., *Jones and Anderson*, 1986; *Anderson et al*., 2010]. Pacific water, during transit across the shallow Bering and Chukchi Sea shelves in winter, interacts with organic-rich sediments and carries nutrients and DIC derived from OM remineralization off-shelf [e.g., *Cooper et al*., 1997; *Nishino et al*., 2005; *Yamamoto-Kawai et al*., 2006; *Anderson et al*., 2010]. If the nutrient and DIC maxima are both derived from remineralization of OM, a comparison of concentrations in PSW and PWW should reflect the stoichiometry of marine OM (DIC/P = 106), and the isotopic composition of DIC should reflect a biological fractionation signature. In addition, AOU, a tracer used to estimate the removal of oxygen by remineralization of OM [*Sarmiento and Gruber*, 2006], should likewise reflect the stoichiometry of remineralization.

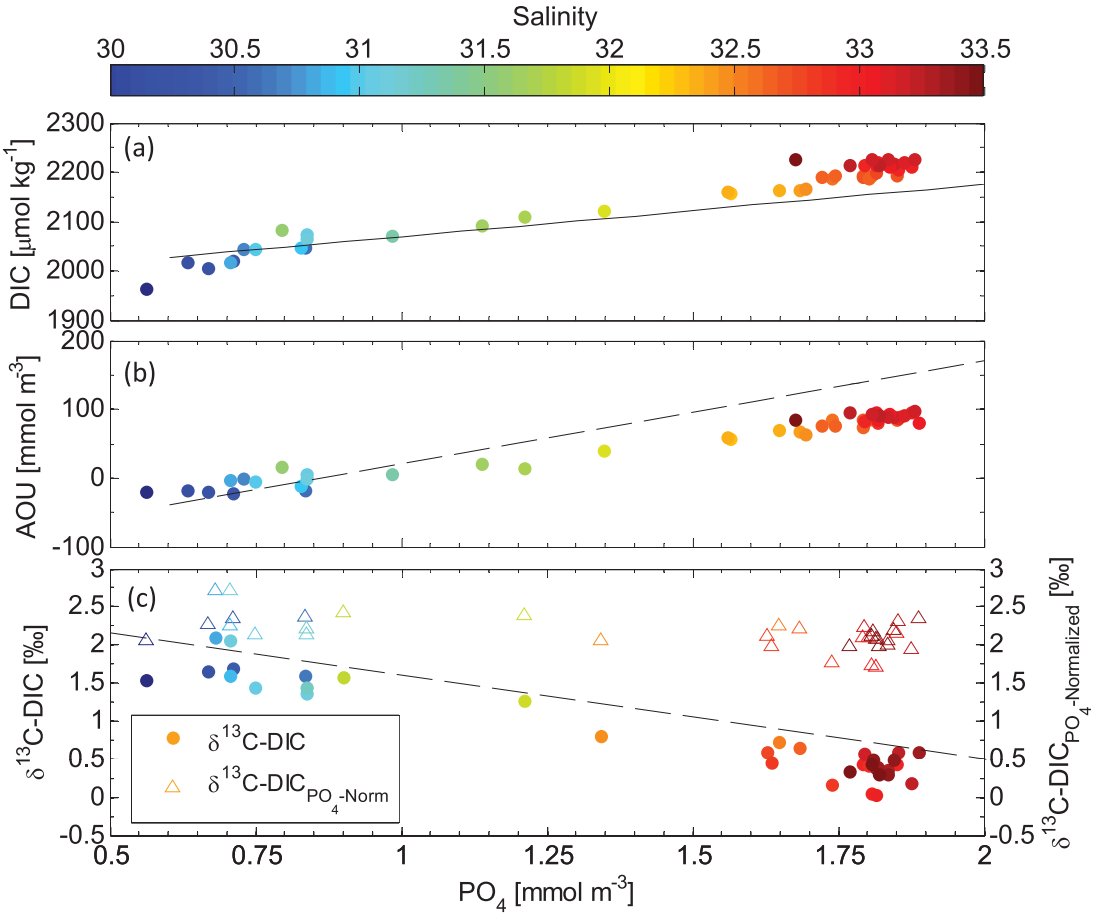

Figure 5. Geochemical properties of the upper and middle halocline in the Canada Basin (PSW layer to PWW layer; $30.0 < S < 33.5$) plotted versus PO_4. The symbol color represents sample salinity as shown on the color scale on top of Figure 5a. Lines in Figures 5a and 5b represent the marine OM relationships of 106:1 for DIC:PO_4 (solid line) and 150:1 for AOU:PO_4 (dashed line), respectively, following *Sarmiento and Gruber* [2006]. Filled circles in Figure 5c denote measured values whereas hollow triangles indicate δ^{13}C-DIC has been normalized to PO_4 ($\delta^{13}C\text{-}DIC_{PO4Normalized}$) following *Charles and Fairbanks* [1990]. The dashed line in Figure 5c represents the δ^{13}C-DIC versus PO_4 relationship determined by *Broecker and Maier-Reimer* [1992]: $\delta^{13}C\text{-}DIC = 2.7 - 1.1 * PO_4$.

5.2.1. C:AOU:P Stoichiometry in the Canada Basin Halocline

Our observations illustrate that DIC and AOU increase with PO_4 between PSW and PWW (Figures 5a and 5b) suggesting increased concentrations of both are likewise related to PO_4 remineralization. However, neither the DIC nor AOU increase follow "classic" marine OM remineralization stoichiometries (106:1 for DIC:PO_4 and −150:1 for AOU:PO_4) [*Anderson*, 1995]. Instead, the DIC increase follows a 160:1 slope as PO_4 increases, resulting in a significant excess of DIC in the higher-salinity range of PWW (Figure 5a). This suggests a non-Redfield or abiotic DIC input (e.g., sea ice or air-sea gas exchange). In contrast, calculated AOU values follow a 90:1 slope as PO_4 increases, which is much lower than the expected 150:1 AOU:PO_4 ratio (Figure 5b). This suggests mixing and/or air-sea gas exchange may have increased oxygen concentrations (and thus decreased the apparent O_2 deficit) in PWW, or that these waters are influenced by anoxic shelf sediment OM remineralization pathways, such as denitrification, which would increase PO_4 without O_2 consumption. Calculated values of AOU and DIC_{diseq} (Figures 4b and 4d), however, show a strong correspondence over the halocline, suggesting similar controls on both O_2 and CO_2 behavior in PSW and PWW layers (AOU versus DIC_{diseq}, $r^2 = 0.77$).

This deviation from "classic" C:AOU:P stoichiometry may indicate the influence of abiotic nonconservative inputs of DIC and O_2 to PWW (investigated below) or that phytoplankton in the Bering and Chukchi Seas do not take up inorganic nutrients in "classic" Redfield/Anderson proportions. Considerable variability has been observed in OM formation and remineralization stoichiometry across the global oceans [e.g., *Martiny et al.*, 2013; *DeVries and Deutsch*, 2014] and in the Arctic Ocean in particular [e.g., *Daly et al.*, 1999;

Thingstad et al., 2008], suggesting the assumption that remineralization products will follow the canonical Redfield/Anderson C:N:P:O_2 ratio of 106:16:1:−150 may not be applicable in all marine environments. A recent Chukchi Shelf study by *Mills et al*. [2015] reported average C:P uptake ratios of ≈96:1 and ≈65:1 in 2010 and 2011, respectively (with a range of observations from 47:1 to 125:1), which are much lower than the ≈160:1 indicated by our PSW and PWW data. If *Mills et al*. [2015] data represent the stoichiometry of remineralization for Canada Basin halocline water, an even greater abiotic DIC and O_2 input is required to reach our observed values. Therefore, although the positive relationship between both DIC and AOU to increasing PO_4 concentrations suggests OM remineralization is the major contributor of nutrients and DIC to shelf-derived PWW, the departure from the expected marine OM remineralization stoichiometry warrants further investigation (section 5.4).

5.2.2. Stable Isotope Signature of DIC Sources

Stable carbon isotope data can be used to provide additional constraints on the sources of DIC to PWW. Modern δ^{13}C-DIC distributions in the interior ocean are dominated by biological fractionation [*Schmittner et al*., 2013], resulting in an inverse relationship between deep water δ^{13}C-DIC and nutrient accumulation from OM remineralization [*Kroopnick*, 1985; *Broecker and Maier-Reimer*, 1992]. Measured δ^{13}C-DIC in the northern North Pacific and Bering Sea has been shown to be largely controlled by biological activity and upwelling/deep water mixing [*Tanaka et al*., 2003], suggesting that δ^{13}C-DIC values in PSW and PWW would be tightly coupled with nutrients if OM remineralization were the main contributor of DIC. Using our δ^{13}C-DIC data, we examined the relationship between nutrient concentrations and stable C isotopes in the Canada Basin halocline (Figure 5c) and found a close correspondence between δ^{13}C-DIC depletion and PO_4 enrichment between the PSW and PWW layers.

Broecker and Maier-Reimer [1992] derived an approximation for the dependence of δ^{13}C-DIC on PO_4, based on mean ocean nutrient and OM composition (equation (14), as modified by *Lynch-Stieglitz et al*. [1995]):

$$\delta^{13}C\text{-}DIC = 2.7 - 1.1 \times PO_4 \tag{14}$$

The slope of this relationship roughly matches with our observations from the southwestern Canada Basin (dashed line Figure 5c, circles; slope = -1.17 ± 0.06, $r^2 = 0.91$), although our values in PWW are consistently isotopically lighter. This offset could reflect regional differences between the Arctic and the mean global oceans. *Charles and Fairbanks* [1990] also used a stoichiometric relationship of [δ^{13}C:PO_4org]:DIC ≈ 0.93‰/μmol kg^{-1} [*Broecker and Peng*, 1982] and postulated that normalizing δ^{13}C-DIC to PO_4 should produce constant values if remineralization of OM was the only control on δ^{13}C-DIC distributions (equation (15)):

$$\delta^{13}C\text{-}DIC_{Norm} = \delta^{13}C\text{-}DIC + (0.93 \times PO_4) \tag{15}$$

Indeed, our observations show that normalizing δ^{13}C-DIC values from PSW and PWW nearly eliminates the dependence on PO_4 concentration (Figure 5c, triangles; slope = -0.24 ± 0.06, $r^2 = 0.29$, not shown). The strong correlation between δ^{13}C-DIC and PO_4, and near-constant values of PO_4-normalized δ^{13}C-DIC (2.16 ± 0.22‰), provide additional evidence that OM remineralization is the dominant contributor of both DIC and PO_4 to PWW.

5.2.3. Advected DIC and Nutrient Contributions to PWW

Other processes could also contribute to the increased nutrient and DIC concentrations in PWW, for example, winter transport of high-nutrient Bering Sea water could account for nutrient and DIC concentrations, without requiring the addition of nutrients from the Chukchi Shelf [*Cooper et al*., 1997]. *Cooper et al*. [1997] determined that typical PWW nutrient concentrations (N ≈ 20 μM; Si ≈ 45 μM; as defined by *Macdonald et al*. [1989]) could be found along the northern Bering Sea slope, in particular, the Gulf of Anadyr, at depths less than 100 m. Although these different sources cannot be distinguished using DIC and PO_4 alone (Figure 5), geochemical tracers such as N* (a measure of denitrification) can provide information on the relative contribution of shelf-derived versus imported nutrients to waters flowing northward along the Bering and Chukchi Sea shelves toward the Canada Basin.

Denitrification (i.e., NO_3^- reduction to N_2) is a well-documented feature of waters found above anaerobic Bering and Chukchi Sea shelf sediments [e.g., *Devol et al*., 1997; *Nishino et al*., 2005; *Yamamoto-Kawai et al*., 2006, 2008]. Strong nitrate depletion (negative N*; Figure 4c) was observed in the southwestern Canada Basin PWW and N* values were lower in PWW (-11.4 ± 0.4 mmol m^{-3}) than in PSW (-8.7 ± 0.8 mmol m^{-3}) in our study (Figure 4c). Average N* values associated with the nutrient maximum (−12.03 and

-11.23 mmol m^{-3} in 2008 and 2009, respectively; Table 3) compare well with N* values reported by *Granger et al*. [2013] for the Gulf of Anadyr, the region thought to be the predominant source of NO_3^- to the Chukchi Sea [*Walsh et al*., 1989]. *Granger et al*. [2013] report N* values in the range of -6 to -12 μM associated with high-nutrient values ($[NO_3^-] \sim 12$ to 20 μM) in bottom waters (50–100 m depth). They further calculated that between 20 and 100% of the NO_3^- associated with winter waters on the inner Bering Sea shelf (south of Bering Strait) was derived from OM remineralization directly on the shelf [*Granger et al*., 2013]. These authors observed a striking decrease in N* (≈ -6 to -13 μmol L^{-1}) and NO_3^- ($\approx$25 to <5 μmol L^{-1}) as bottom waters moved northward from the slope toward Bering Strait, suggesting that advection of these waters could be a source of highly depleted N* PWW to the Chukchi Sea and onward to the Canada Basin.

Nitrogen cycle observations from the Chukchi Shelf and Canada Basin by *Brown et al*. [2015] also illustrate that sediment remineralization is a substantial contributor to the Canada Basin halocline. These authors calculate that at least 58% of the NO_3^- in PWW was regenerated as a result of sediment OM remineralization, specifically NH_4^+ nitrification, during transit across the Chukchi Shelf. Depending on the stoichiometric ratio we use, this could account for between one third (57 μmol kg^{-1}; C:N = 6.6) to one half (86 μmol kg^{-1}; C:N = 10) of the DIC increase between the average PSW (2050 μmol kg^{-1}) and the DIC maximum (2226 μmol kg^{-1}; Table 4).

Work by *Brown et al*. [2015] provides strong evidence that the nutrient maximum in the Canada Basin is sourced primarily from OM remineralization within the sediments of the Chukchi Sea. Although our inorganic carbon, nutrient, and stable isotope tracer comparisons between PSW and PWW also suggest a strong control of OM remineralization on the DIC maxima in the Canada Basin halocline, the non-Redfield/Anderson stoichiometry of the increase in DIC: P of PWW when compared to the DIC:P of PSW suggests other abiotic sources of DIC may also contribute to the high concentrations found in these waters.

5.3. Processes That Change DIC Without Altering Nutrient Inventories

Non-Redfield stoichiometry of DIC:AOU:PO_4 additions to PWW could be explained by nonconservative, abiotic DIC contributions to PWW. These include air-sea gas exchange and sea-ice brine rejection in the Bering/Chukchi region, processes that change DIC without altering nutrient inventories.

5.3.1. Air-Sea Gas Exchange

Exchange of CO_2 between the surface ocean and the atmosphere is a process that can strongly decouple δ^{13}C-DIC from nutrient concentrations and AOU [*Charles and Fairbanks*, 1990]. Atmosphere-ocean δ^{13}C equilibration is temperature dependent, and given sufficient time, results in an isotopic enrichment of polar surface waters [*Mook et al*., 1974; *Zhang et al*., 1995]. Isotopic equilibration between CO_2 in the atmosphere and the oceanic pool of DIC is slow ($\approx$10 years for a 50 m mixed layer), however, and equilibrium is never actually achieved [*Lynch-Stieglitz et al*., 1995]. Incomplete equilibration between the ocean and the atmosphere results in a depletion of surface δ^{13}C-DIC in subpolar regions, where cooling increases CO_2 solubility and enhances atmospheric CO_2 uptake [*Broecker and Maier-Reimer*, 1992; *Lynch-Stieglitz et al*., 1995; *Schmittner et al*., 2013]. In contrast, CO_2 outgassing enriches surface water δ^{13}C-DIC until equilibrium is achieved (due to preferential loss of the lighter isotopic species) [*Lynch-Stieglitz et al*., 1995].

We can evaluate the possibility of changes in DIC due to CO_2 uptake or degassing at the air-sea interface as Pacific waters transit seasonally across the Chukchi Shelf by calculating DIC_{diseq} (Figure 4d). Waters in the southwestern Canada Basin had an excess DIC of up to $\approx$90 μmol kg^{-1} in the PWW layer during our study, whereas the PSW layer showed a deficit in DIC (Figure 4d). This implies PWW is significantly oversaturated with respect to atmospheric CO_2 and thus would lose CO_2 to the atmosphere if they come to the surface. During transit to the Canada Basin, any out-gassing of CO_2 from these waters to the atmosphere would isotopically enrich DIC remaining in solution. Annual mean transit times between Bering Strait and the head of Barrow Canyon suggest the residence time of Pacific water in the Chukchi Sea is on the order of 3–6 months [*Woodgate and Aagaard*, 2005; *Woodgate et al*., 2005; *Cai et al*., 2014] and therefore high pCO_2 Pacific waters transiting the shallow Bering and Chukchi Sea shelves in winter are limited in their ability to lose CO_2 to the atmosphere, especially under the intermittent cover of ice.

In contrast, at the end of summer, waters on the Bering and Chukchi Shelves have been shown to be pCO_2 undersaturated with respect to the atmosphere [e.g., *Bates*, 2006; *Semiletov et al*., 2007]. Cooling of these waters over the winter would further increase CO_2 solubility, promoting CO_2 uptake during transit. This scenario is unlikely to produce partial pressures of CO_2 higher than atmospheric values, unless waters warm

again. Although Figure 5b suggests oxygen uptake from the atmosphere may have contributed to lower AOU in PWW, air-sea exchange of oxygen in waters transiting the Bering and Chukchi Seas has been observed to be of relatively minor importance compared to remineralization/recycling of OM and dilution by sea-ice melt [*Cooper et al*., 1999]. This suggests the impact of air-sea exchange on DIC is even more limited, as air-sea equilibration of CO_2 takes ≈20 times longer than oxygen due to the buffered solution chemistry of DIC (as summarized in *Sarmiento and Gruber* [2006]). The high positive DIC_{diseq} values in the PWW layer, coupled with a δ^{13}C-DIC signature isotopically lighter than that of PSW (Figure 2c), indicate that air-sea gas exchange is not an important contributor to the DIC maximum in the south-western Canada Basin halocline. The apparent deficit in AOU:PO_4 in these waters, however, suggests that even if air-sea exchange is of minor importance, sea-ice formation, deep mixing, and winter cooling may contribute enough to the oxygenation of PWW to decouple AOU from PO_4.

5.3.2. Sea-Ice Formation and Brine Rejection

The contribution of high-salinity brine to the water column during sea-ice formation (negative f_{SIM}) is a distinctive feature of the Canada Basin halocline, observed in both PSW and PWW layers, and extending into the ATW layer (Figure 2d) [*Yamamoto-Kawai et al*., 2008; *McLaughlin et al*., 2011]. While the conservative increase in DIC concentrations with increasing S in forming brines is accounted for in the normalization of DIC to S = 35, the precipitation of solid carbonate salts ($CaCO_3$) within forming sea ice will alter DIC_{norm} and could be coupled with the nonconservative addition of CO_2 to surface waters via diffusion [*Rysgaard et al*., 2007]. Solid salt precipitation will also be associated with the fractionation of ^{13}C into isotopically heavy $Ca^{13}CO_3$ and isotopically light $^{13}CO_2$ [*Romanek et al*., 1992; *Papadimitriou et al*., 2004], which could result in brine with a differing δ^{13}C-DIC signature compared to parent seawater. Thus, brine injected into the water column during sea-ice formation could contribute isotopically light δ^{13}C-DIC and an increased ratio of DIC/TAlk to surface waters if isotopically heavy $CaCO_3$ (TAlk) were retained within the forming sea ice. Even without brine export, diffusion of isotopically light $^{13}CO_2$ from brine channels to surface waters could deplete δ^{13}C-DIC compared to pre-ice conditions.

Although Figure 5c provides strong evidence that organic matter remineralization is the dominant contributor of both DIC and PO_4 to the PWW layer, DIC added to under-ice waters by CO_2 diffusion may contribute to the noise around the average isotopic signature of the PWW layer. We can estimate the isotopic composition of this DIC from the temperature-independent fractionation factors for aragonite and calcite ($\varepsilon_{CaCO3\text{-}HCO3\text{-}} = +2.7‰$ and $+1.0‰$, respectively) [*Romanek et al*. 1992], which would give DIC with an isotopic signature on the order of $-0.34‰$ (taking the $+1.51‰$ average for PSW minus the average fractionation factor of $+1.85‰$ for calcite and aragonite). Using a simplistic mass balance equation (equation (16)), we can calculate the DIC (CO_2) that would be needed to bring the isotopic signature of PSW to that measured in the PWW layer.

$$\begin{aligned} &DIC_{PWW}\,(\mu mol\,kg^{-1}) \times \delta^{13}C\,DIC_{PWW}\,(‰) \\ &= DIC_{PSW}\,(\mu mol\,kg^{-1}) \times \delta^{13}C\,DIC_{PSW}\,(‰) + DIC_{Brine}\,(\mu mol\,kg^{-1}) \times \delta^{13}C\,DIC_{Brine}\,(‰) \end{aligned} \tag{16}$$

Here DIC_{Brine} refers to the DIC added to surface waters by diffusion of CO_2 from $CaCO_3$ precipitation within the brine channel network ($Ca^{2+} + 2HCO_3^- \Longleftrightarrow CaCO_3 + CO_2 + H_2O$). Average values for PWW DIC and δ^{13}C-DIC are taken from Table 4; PSW DIC and δ^{13}C-DIC are taken as the average measured values between $30.3 < S < 31.5$ (2048 μmol kg^{-1} and $+1.51‰$, respectively; Figures 2b and 2c).

If all other contributions of DIC to PWW are ignored (e.g., air-sea CO_2 exchange and the DIC increase associated with conservative concentration in sea-ice brines), our mass balance indicates that ≈6400 μmol kg^{-1} of CO_2 (derived from $CaCO_3$ precipitation) would need to diffuse into PSW from overlying sea ice to account for the isotopic signature measured in PWW. This value is almost an order of magnitude greater than $CaCO_3$ precipitation previously reported in Arctic sea ice. For example, *Rysgaard et al*. [2013] measured $CaCO_3$ concentrations in winter sea ice on the order of 100–900 μmol kg^{-1}. While this calculation does not unequivocally rule out some CO_2 contribution to surface waters from $CaCO_3$ precipitation in sea ice, it confirms that this process is of minor importance to the PWW DIC budget.

5.4. A Basic Model for PSW and PWW Nutrient and DIC Content

The previous analysis indicates that abiotic nonconservative sources of DIC are not important contributors to the DIC maximum observed in the Canada Basin halocline. How then can we explain the deviation of

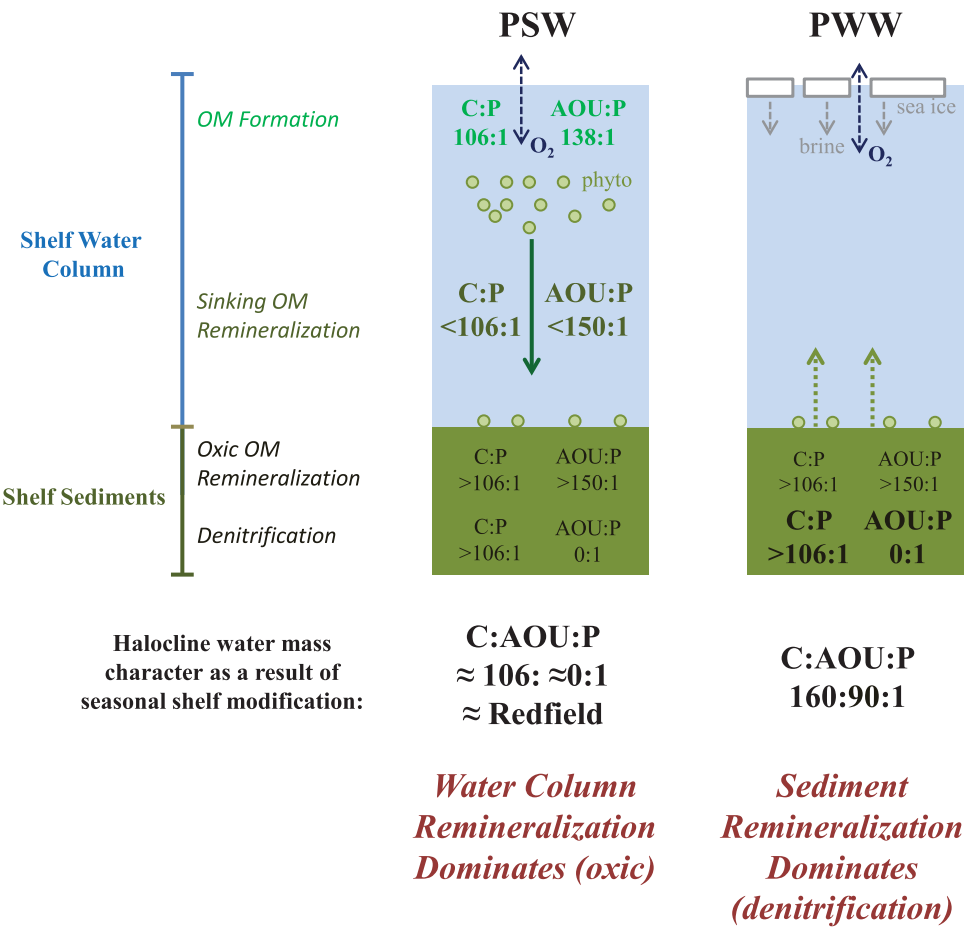

Figure 6. A basic model for PSW and PWW nutrient and DIC content (see section 5.4 for details). The left-hand plot illustrates the transformations of OM within the sediments and the water column as Pacific waters transit the shallow shelves in summer (PSW), and the right-hand column illustrates OM transformations during winter transit (PWW). Seasonal shelf modification of transiting Pacific waters results in predominantly water column nutrient + DIC uptake/remineralization dominating in the summer and sediment remineralization processes dominating in the winter, impacting the C:AOU:P of PSW and PWW, respectively.

C:AOU:P from the expected OM remineralization stoichiometry of 106:−150:1 (Figures 5a and 5b) if the main source of DIC and nutrients to PWW is OM remineralization? We invoke a hypothesis to explain this deviation that relies on the seasonal separation of Pacific waters as they transit the Bering/Chukchi shelves in summer and winter on a time scale of 3–6 months [*Woodgate and Aagaard*, 2005; *Woodgate et al*., 2005; *Cooper et al*., 1997].

Waters transiting the shelves in summer will experience high primary productivity (Figure 6). Organic material in summer water should form following Redfield stoichiometry (C:AOU:P = 106:−138:1), or lower stoichiometry reported by *Mills et al*., [2015] (C:P of ≈96:1 and ≈65:1), and some of this material will be remineralized in the water column as it sinks. As P is preferentially remineralized over C [*Clark et al*., 1998; *Paytan et al*., 2003], the remineralization products will have a <106:1 C:P ratio, leaving the OM that makes it to the sediments with a >106:1 C:P ratio. As water column remineralization is oxygen consuming, AOU:P should reflect Redfield/Anderson stoichiometry (−150:1 or slightly lower to account for the lower C:P), but O_2 addition during photosynthesis and air-sea gas exchange will keep O_2 near atmospheric equilibrium, yielding PSW AOU ≈ 0 (Figure 6a). From our observations (Figures 5a and 5b), the C:AOU:P of PSW in the Canada Basin halocline appears to predominantly reflect this water column remineralization signature, with oxygen addition from photosynthesis and/or air-sea exchange.

In winter, no new OM is produced in the upper water column, so remineralization in the sediments underlying winter water becomes the main source of remineralized C and nutrients, yielding a C:P > 106/1. In addition, denitrification in the sediments will have a greater impact on deeply mixed water that interacts with

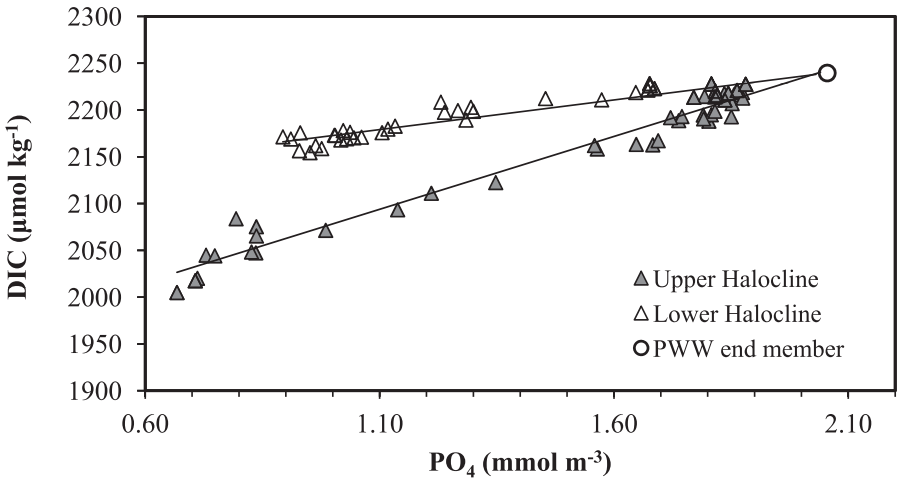

Figure 7. Plot of DIC versus PO_4 within the Canada Basin halocline, measured values from the upper halocline (PSW layer to PWW layer) are illustrated with filled symbols, whereas values from the lower halocline (PWW layer to ATW) are illustrated with open symbols. Linear regression lines through the data converge at a hypothetical PWW "end-member" (open circle).

shelf sediments during transit, accounting for their higher N* and the decoupling between AOU and P, since a fraction of OM remineralization in sediment does not use O_2 as electron acceptor. Addition of O_2 to the cooling water column by atmospheric equilibration could further reduce AOU:P (Figure 6b). This seasonal separation of Pacific water transiting the shelves can explain the higher C:P and lower AOU:P ratios in PWW compared to PSW found in the Canada Basin halocline. Water column remineralization (oxic) of OM and oxygen production/exchange dominates PSW C:AOU:P, whereas sediment remineralization of high C:P OM (including denitrification, decoupling C:AOU:P) dominates PWW stoichiometry.

5.5. The Nutrient and DIC Maxima Mismatch

While our analysis identifies the dominant remineralization sources of DIC to the PWW layer, the differences between the S signature of the nutrient maximum and the DIC maximum (Figure 3) requires further explanation. As discussed below, our observations suggest that physical mixing between end-member water masses in the halocline can be invoked to explain the different S ranges of the nutrient and DIC maxima.

Figure 7 illustrates DIC and PO_4 concentrations within the upper halocline (PSW layer to PWW layer; filled triangles) and the lower halocline to the depth of the ATW T-maximum (PWW to ATW layer; open triangles). Regression lines through each of the halocline subsections generate mixing lines between both PSW and ATW with a hypothetical PWW end-member (open circle; Figure 7), generated as a result of sea-ice brine rejection on the Chukchi Shelf. The difference in slope seen between the PSW-PWW and the PWW-ATW lines illustrate that DIC concentrations in ATW core are almost as high as the PWW layer. Due to the smaller DIC gradient between PWW and ATW, mixing will have less of an impact on DIC than on PO_4, and this translates into a larger S range for the DIC maximum, relative to the PO_4 maximum (cf. Tables 3 and 4). Mixing of these water masses explains the differences between the S of the maximum PO_4 and DIC values shown in Figures 3 and 4a.

6. Conclusions

Using nutrient and inorganic carbon tracers, stable carbon isotopes, and AOU, we investigated the contribution of various processes to the formation of the DIC maximum in the southwestern Canada Basin halocline. This investigation has illustrated that once conservative contributions are accounted for, the nutrient and DIC maxima in the PWW layer are predominantly derived from the products of OM remineralization within Bering and Chukchi Sea sediments, which are entrained in northward flowing Pacific Winter Waters as they are seasonally modified on the shelves and delivered to the deep basin. Mixing between PWW and ATW in the lower halocline explains the differences between the S fingerprints of the DIC maximum ($S = 33.0$–33.58) and PO_4 maximum ($S \approx 33.0$), because DIC concentrations are similar between the two water masses, whereas PO_4 is much lower in ATW.

Our analysis also indicates that air-sea gas exchange and nonconservative contributions of CO_2 associated with $CaCO_3$ precipitation during sea-ice formation are not important sources of DIC to the Canada Basin halocline. Despite the negligible impacts of these surface processes on the DIC content of the PWW layer, the continental shelf CO_2-pump associated with sea-ice formation is still the main driver for the delivery of surface water CO_2 to the halocline [e.g., *Anderson et al*., 2010] and this process may be sensitive to a warming Arctic climate. Additionally, this pump acts to maintain the CO_2 undersaturation of shelf waters in contact with the atmosphere that persists throughout the ice-covered winter months [*Anderson et al*., 2010]. Increased production of new winter sea ice (resulting from a greater fraction of open water at the end of the summer) could result in an increase in the frequency of events that act to ventilate the halocline via the off-shelf transport of dense water flows [e.g., *Weingartner et al*., 1998; *Winsor and Chapman*, 2002; *Shimada*, 2005], potentially increasing the delivery of DIC to the Canada Basin halocline. Counteracting this, however, an increased freshwater flux to the Arctic will increase stratification and decrease shelf water salinity [e.g., *Winsor and Chapman*, 2002] thereby inhibiting the formation of waters dense enough to ventilate the halocline. This, in turn, would reduce the efficiency of the continental shelf CO_2 pump and promote CO_2 efflux along the shelves [e.g., *Anderson et al*., 2010]. Ice edge retreat beyond the shelf break in summer may also promote the upwelling of high DIC waters onto the shallow shelves, potentially contributing to further CO_2 efflux under high wind mixing conditions [*Carmack and Chapman*, 2003]. Future studies examining the impact of changing sea-ice conditions on CO_2 fluxes along the shelf break are required to understand the potential impacts of climate change on the CO_2 source/sink status of the Arctic shelf regions and their contributions to CO_2 sequestration within the deep central basins.

Acknowledgments

We acknowledge support from NSERC, Fisheries and Oceans Canada, the US National Science Foundation Office of Polar Programs (grant OPP-0424864), and the Canadian International Polar Year Office. We thank Chief Scientist Sarah Zimmermann, IOS & WHOI Science personnel, and the captains and crews of the *CCGS Louis S. St. Laurent* for their help with sample collection and support of this field investigation. Special thanks also go to J. F. Hélie and Marty Davelaar for patient help with laboratory analyses and to Maureen Soon for logistical assistance. Finally, we thank an anonymous reviewer for constructive comments that helped to improve our manuscript. Data presented in this publication can be obtained through the WHOI Beaufort Gyre Observation System website, http://www.whoi.edu/beaufortgyre/data.

References

Aagaard, K., and E. C. Carmack (1989), The role of sea ice and other fresh water in the Arctic circulation, *J. Geophys. Res.*, *94*(C10), 14,485–14,498, doi:10.1029/JC094iC10p14485.

Aagaard, K., and E. C. Carmack (1994), The Arctic Ocean and climate: A perspective, in *The Polar Oceans and Their Role in Shaping the Global Environment, Geophys. Monogr. Ser*., vol. 85, pp. 5–20, AGU, Washington, D. C., doi:10.1029/GM085p0005.

Aagaard, K., L. K. Coachman, and E. Carmack (1981), On the halocline of the Arctic Ocean, *Deep Sea Res., Part A*, *28*(6), 529–545.

Anderson, L. A. (1995), On the hydrogen and oxygen content of marine phytoplankton, *Deep Sea Res., Part I*, *42*(9), 1675–1680.

Anderson, L. G., E. P. Jones, R. Lindegren, B. Rudels, and P.-I. Sehlstedt (1988), Nutrient regeneration in cold, high salinity bottom water of the Arctic shelves, *Cont. Shelf Res.*, *8*(12), 1345–1355, doi:10.1016/0278-4343(88)90044-1.

Anderson, L. G., D. Dyrssen, and E. P. Jones (1990), An assessment of the transport of atmospheric CO_2 into the Arctic Ocean, *J. Geophys. Res.*, *95*(89), 1703–1711.

Anderson, L. G., E. Falck, E. P. Jones, S. Jutterström, and J. H. Swift (2004), Enhanced uptake of atmospheric CO_2 during freezing of seawater: A field study in Storfjorden, Svalbard, *J. Geophys. Res.*, *109*, C06004, doi:10.1029/2003JC002120.

Anderson, L. G., T. Tanhua, G. Björk, S. Hjalmarsson, E. P. Jones, S. Jutterström, B. Rudels, J. H. Swift, and I. Wåhlstöm (2010), Arctic ocean shelf–basin interaction: An active continental shelf CO_2 pump and its impact on the degree of calcium carbonate solubility, *Deep Sea Res., Part I*, *57*(7), 869–879, doi:10.1016/j.dsr.2010.03.012.

Bates, N. R. (2006), Air-sea CO_2 fluxes and the continental shelf pump of carbon in the Chukchi Sea ageacent to the Arctic Ocean, *J. Geophys. Res.*, *111*, C10013, doi:10.1029/2005JC003083.

Bates, N. R., M. Best, and D. Hansell (2005), Spatio-temporal distribution of dissolved inorganic carbon and net community production in the Chukchi and Beaufort Seas, *Deep Sea Res., Part II*, *52*(24-26), 3303–3323, doi:10.1016/j.dsr2.2005.10.005.

Bates, N. R., W.-J. Cai, and J. T. Mathis (2011), The ocean carbon cycle in the western Arctic Ocean: Distributions and air-sea fluxes of carbon dioxide, *Oceanography*, *24*(3), 186–201, doi:10.5670/oceanog.2011.71.

Broecker, W. S., and E. Maier-Reimer (1992), The influence of air and sea exchange on the carbon isotope distribution in the sea, *Global Biogeochem. Cycles*, *6*(3), 315–320, doi:10.1029/92GB01672.

Broecker, W. S., and T.-H. Peng (1982), *Tracers in the Sea*, Eldigio, N. Y.

Brown, K. A., F. McLaughlin, P. D. Tortell, D. Varela, M. Yamamoto-Kawai, B. Hunt, and R. François (2014), Determination of particulate organic carbon sources to the surface mixed layer of the central Canada Basin, Arctic Ocean, *J. Geophys. Res. Oceans*,*119*, 1084–1102, doi:10.1002/2013JC009197.

Brown, Z. W., K. L. Casciotti, R. S. Pickart, J. H. Swift, and K. R. Arrigo (2015), Aspects of the marine nitrogen cycle of the Chukchi Sea shelf and Canada Basin, *Deep Sea Res., Part II*, *118*, 73–87, doi:10.1016/j.dsr2.2015.02.009.

Cai, W. J., et al. (2010), Decrease in the CO_2 uptake capacity in an ice-free Arctic Ocean basin, *Science*, *329*, 556–559, doi:10.1126/science.1189338.

Cai, W.-J., N. R. Bates, L. Guo, L. G. Anderson, J. Mathis, R. Wanninkhof, D. A. Hansell, L. Chen, and I. Semiletov (2014), Carbon fluxes across boundaries in the Pacific region in a changing environment, in *The Pacific Arctic Region: Ecosystem Status and Trends in a Rapidly Changing Environment*, edited by J. M. Grebmeier and W. Maslowski, pp. 199–222, Springer, Dordrecht, Netherlands.

Carmack, E., and D. C. Chapman (2003), Wind-driven shelf/basin exchange on an Arctic shelf: The joint roles of ice cover extent and shelf-break bathymetry, *Geophys. Res. Lett.*, *30*, 1778.

Charles, C. D., and R. G. Fairbanks (1990), Glacial to interglacial changes in the isotopic gradients of Southern Ocean surface waters, in *Geological History of the Polar Oceans: Arctic Versus Antarctic*, edited by U. Bleil and J. Thiede, pp. 519–538, Kluwer Acad., Netherlands.

Clark, L. L., E. D. Ingall, and R. Benner (1998), Marine phosphorus is selectivly remineralized, *Nautre*, *393*, 426.

Coachman, L. K., and C. A. Barnes (1961), The contribution of Bering Sea water to the Arctic Ocean, *Arctic*, *14*, 146–161.

Coachman, L. K., K. Aagaard, and R. B. Tripp (1975), *Bering Strait: The Regional Physical Oceanography*, Univ. of Wash. Press, Seattle.

Cooper, L. W., T. E. Whitledge, M. Grebmeier, and T. Weingartner (1997), The nutrient, salinity, and stable oxygen isotope composition of Bering and Chukchi Seas waters in and near the Bering Strait, *J. Geophys. Res.*, *102*(C6), 12,563–12,573.

Cooper, L. W., F. Cota, R. Pomeroy, M. Grebmeier, and T. E. Whitledge (1999), Modification of NO, PO, and NO/PO during flow across the Bering and Chukchi shelves: Implications for use as Arctic water mass tracers, *J. Geophys. Res.*, *104*(C4), 7827–7836.

Cooper, L. W., J. W. McClelland, R. M. Holmes, P. A. Raymond, J. J. Gibson, C. K. Guay, and B. J. Peterson (2008), Flow-weighted values of runoff tracers (δ^{18}O, DOC, Ba, alkalinity) from the six largest Arctic rivers, *Geophys. Res. Lett.*, *35*, L18606, doi:10.1029/2008GL035007.

Daly, K. L., D. W. R. Wallace, W. O. Smith Jr., A. Skoog, R. Lara, M. Gosselin, E. Falck, and P. L. Yager (1999), Non-Redfield carbon and nitrogen cycling in the Arctic: Effects of ecosystem structure and dynamics, *J. Geophys. Res.*, *104*(C2), 3185–3199.

Devol, A. H., L. A. Codispotit, and J. P. Christensen (1997), Summer and winter denitrification rates in western Arctic shelf sediments, *Cont. Shelf Res.*, *17*(9), 1029–1050.

DeVries, T., and C. Deutsch (2014), Large-scale variations in the stoichiometry of marine organic matter respiration, *Nat. Geosci.*, *7*, 890–894, doi:10.1038/NVEO2300.

Dickson, A. G. (1990), Standard potential of the reaction: AgCl (s) + 1/2H,(g) = Ag (s) + HCl (aq), and and the standard acidity constant of the ion HSO_4^- in synthetic sea water from 273.15 to 318.15 K, *J. Chem. Thermodyn.*, *22*, 113–127.

Dickson, A. G., and F. J. Millero (1987), A comparison of the equilibrium constants for the dissociation of carbonic acid in seawater media, *Deep Sea Res., Part A*, *34*(111), 1733–1743.

Dickson, A. G., C. L. Sabine, and J. R. Christian (Eds.) (2007), *Guide to best practices for ocean CO_2 measurements, PICES Special Publication 3*, 191 pp.

Epstein, S., and T. Mayeda (1953), Variation of O_{18} content of waters from natural sources, *Geochim. Cosmochim. Acta*, *4*, 213–224.

Friis, K., A. Kortzinger, and D. W. R. Wallace (2003), The salinity normalization of marine inorganic carbon chemistry data, *Geophys. Res. Lett.*, *30*(2), 1085, doi:10.1029/2002GL015898.

Granger, J., M. G. Prokopenko, C. W. Mordy, and D. M. Sigman (2013), The proportion of remineralized nitrate on the ice-covered eastern Bering Sea shelf evidenced from the oxygen isotope ratio of nitrate, *Global Biogeochem. Cycles*, *27*, 962–971, doi:10.1002/gbc.20075.

Gruber, N., and J. L. Sarmiento (1997), Global patterns of marine nitrogen fixation and denitrification, *Global Biogeochem. Cycles*, *11*(2), 235–266.

Guo, L., Y. Cai, C. Belzile, and R. W. Macdonald (2012), Sources and export fluxes of inorganic and organic carbon and nutrient species from the seasonally ice-covered Yukon River, *Biogeochemistry*, *107*(1-3), 187–206, doi:10.1007/s10533-010-9545-z.

IUPAC (1997), *Compendium of Chemical Terminology*, 2nd ed., Blackwell Sci., Oxford, U. K., doi:10.1351/goldbook.

Jones, E., and L. Anderson (1986), On the origin of the chemical properties of the Arctic Ocean halocline, *J. Geophys. Res.*, *91*(6), 10,759–10,767.

Jones, E. P., L. G. Anderson, and J. H. Swift (1998), Distribution of Atlantic and Pacific waters in the upper Arctic Ocean: Implications for circulation distinguish between oceanic waters of Pacific, *Geophys. Res. Lett.*, *25*(6), 765–768.

Kaltin, S., and L. G. Anderson (2005), Uptake of atmospheric carbon dioxide in Arctic shelf seas: Evaluation of the relative importance of processes that influence pCO_2 in water transported over the Bering–Chukchi Sea shelf, *Mar. Chem.*, *94*(1-4), 67–79, doi:10.1016/j.marchem.2004.07.010.

Kroopnick, P. M. (1985), The distribution of ^{13}C of $\sum CO_2$ in the world oceans, *Deep Sea Res., Part A*, *32(I)*, 57–84.

Loose, B., L. Miller, S. Elliot, and T. Papakyriakou (2011), Sea ice biogeochemistry and material transport across the frozen interface, *Oceanography*, *24*(3), 202–218, doi:10.5670/oceanog.2011.72.

Lynch-Stieglitz, J., T. F. Stocker, W. S. Broecker, and R. G. Fairbanks (1995), The influence of air-sea exchange on the isotopic composition of oceanic carbon: Observations and modeling, *Global Biogeochem. Cycles*, *9*(4), 653–665.

Macdonald, R., E. C. Carmack, F. A. McLaughlin, K. Iseki, D. M. Macdonald, and M. C. O'Brien (1989), Composition and modification of water masses in the Mackenzie Shelf Estuary, *J. Geophys. Res.*, *94*(C12), 18,057–18,070.

Martiny, A. C., C. T. A. Pham, F. W. Primeau, J. A. Vrugt, J. K. Moore, S. A. Levin, and M. W. Lomas (2013), Strong latitiduinal patters in the elemental ratios of marine plankton and organic matter, *Nat. Geosci.*, *6*, 279–283, doi:10.1038/ngeo1757.

McLaughlin, F. A., and E. C. Carmack (2010), Deepening of the nutricline and chlorophyll maximum in the Canada Basin interior, 2003-2009, *Geophys. Res. Lett.*, *37*, L24602, doi:10.1029/2010GL045459.

McLaughlin, F. A., E. C. Carmack, R. W. Macdonald, H. Melling, J. H. Swift, P. Wheeler, B. Sherr, and E. Sherr (2004), The joint roles of Pacific and Atlantic-origin waters in the Canada Basin, 1997–1998, *Deep Sea Res., Part I*, *51*(1), 107–128, doi:10.1016/j.dsr.2003.09.010.

McLaughlin, F. A., E. C. Carmack, A. Proshutinsky, R. A. Krishfield, C. Guay, M. Yamamoto-Kawai, J. M. Jackson, and B. Williams (2011), The rapid response of the Canada Basin to climate forcing: From bellwether to alarm bells, *Oceanography*, *24*(3), 146–159.

McLaughlin, F. A., et al. (2012), Physical, chemical and zooplankton data from the Canada Basin and Canadian Arctic Archipelago, July 20 to September 14, 2006, *Can. Data Rep. Hydrogr. Ocean Sci. 186*, Fisheries and Oceans Science Branch, Pacific Region, Sidney, British Columbia, Canada.

Mehrbach, C., C. H. Culberson, J. E. Hawley, and R. M. Pytkowicz (1973), Measurement of the apparent dissociation constants of carbonic acid in seawater at atmospheric pressure, *Limnol. Oceanogr.*, *18*(6), 897–907.

Melling, H., and E. L. Lewis (1982), Shelf drainage flows in the Beaufort Sea and their effect on the Arctic Ocean pycnocline, *Deep Sea Res., Part A*, *29*(8), 967–985, doi:10.1016/0198-0149(82)90021-8.

Melling, H., and R. M. Moore (1995), Modification of halocline source waters during freezing on the Beaufort Sea shelf: Evidence from oxygen isotopes and dissolved nutrients, *Cont. Shelf Res.*, *15*(1), 89–113.

Miller, L. A., T. N. Papakyriakou, R. E. Collins, J. W. Deming, J. K. Ehn, R. W. Macdonald, A. Mucci, O. Owens, M. Raudsepp, and N. Sutherland (2011), Carbon dynamics in sea ice: A winter flux time series, *J. Geophys. Res.*, *116*, C02028, doi:10.1029/2009JC006058.

Mills, M. M., et al. (2015), Impacts of low phytoplankton NO_3^-:PO_4^{3-} utilization ratios over the Chukchi Shelf, Arctic Ocean, *Deep Sea Res., Part II*, *118*, 105–121, doi:10.1016/j.dsr2.2015.02.007.

Mook, W., J. Bommerson, and W. Staverman (1974), Carbon isotope fractionation between dissolved bicarbonate and gaseous carbon dioxide, *Earth Planet. Sci. Lett.*, *22*, 169–176.

Moore, R., M. Lowings, and F. Tan (1983), Geochemical profiles in the central Arctic Ocean: Their relation to freezing and shallow circulation, *J. Geophys. Res.*, *88*(C4), 2667–2674.

Murata, A., and T. Takizawa (2003), Summertime CO_2 sinks in shelf and slope waters of the western Arctic Ocean, *Cont. Shelf Res.*, *23*(8), 753–776, doi:10.1016/S0278-4343(03)00046-3.

Newton, R., P. Schlosser, R. Mortlock, J. Swift, and R. MacDonald (2013), Canadian Basin freshwater sources and changes: Results from the 2005 Arctic Ocean Section, *J. Geophys. Res. Oceans*, *118*, 2133–2154, doi:10.1002/jgrc.20101.

Nishino, S., K. Shimada, and M. Itoh (2005), Use of ammonium and other nitrogen tracers to investigate the spreading of shelf waters in the western Arctic halocline, *J. Geophys. Res.*, *110*, C10005, doi:10.1029/2003JC002118.

Omar, A., T. Johannessen, R. G. J. Bellerby, A. Olsen, L. G. Anderson, and C. Kivimae (2005), Sea-ice and brine formation in Storjgorden: Implications for the Arctic wintertime air-sea CO_2 flux, in *The Nordic Seas: An Integrated Perspective*, edited by and W. B. H. Drange et al., pp. 177–187, AGU, Washington, D. C.

Östlund, H. G., and G. Hut (1984), Arctic Ocean water mass balance from isotope data, *J. Geophys. Res.*, *89*(C4), 6373–6381, doi:10.1029/JC089iC04p06373.
Papadimitriou, S., H. Kennedy, G. Kattner, G. S. Dieckmann, and D. N. Thomas (2004), Experimental evidence for carbonate precipitation and CO_2 degassing during sea ice formation, *Geochim. Cosmochim. Acta*, *68*(8), 1749–1761, doi:10.1016/j.gca.2003.07.004.
Paytan, A., B. J. Cade-Menun, K. McLaughlin, and K. L. Faul (2003), Selective phosphorus regeneration of sinking marine particles: Evidence from ^{31}P-NMR, *Mar. Chem.*, *82*, 55–70.
Pierrot, D., E. Lewis, and D. W. R. Wallace (2006), MS Excel program developed for CO_2 system calculations, ORNL/CDIAC-105a, Carbon Dioxide Inf. Anal. Cent., Oak Ridge Natl. Lab., Oak Ridge, Tenn.
Proshutinsky, A. (2002), The role of the Beaufort Gyre in Arctic climate variability: Seasonal to decadal climate scales, *Geophys. Res. Lett.*, *29*(23), 2100, doi:10.1029/2002GL015847.
Romanek, C. S., E. L. Grossman, and J. W. Morse (1992), Carbon isotopic fractionation in synthetic aragonite and calcite: Effects of temperature and precipitation rate, *Geochim. Cosmochim. Acta*, *56*(1), 419–430, doi:10.1016/0016-7037(92)90142-6.
Rysgaard, S., R. N. Glud, M. K. Sejr, J. Bendtsen, and P. B. Christensen (2007), Inorganic carbon transport during sea ice growth and decay: A carbon pump in polar seas, *J. Geophys. Res.*, *112*, C03016, doi:10.1029/2006JC003572.
Rysgaard, S., J. Bendtsen, B. Delille, G. S. Dieckmann, R. N. Glud, H. Kennedy, J. Mortensen, S. Papadimitriou, D. N. Thomas, and J.-L. Tison (2011), Sea ice contribution to the air-sea CO_2 exchange in the Arctic and Southern Oceans, *Tellus, Ser. B*, *63*(5), 823–830, doi:10.1111/j.1600-0889.2011.00571.x.
Rysgaard, S., D. H. Søgaard, M. Cooper, M. Pucko, K. Lennert, T. N. Papakyriakou, F. Wang, N. X. Geilfus, R. N. Glud, J. Ehn, D. F. McGinnis, K. Attard, J. Sievers, J. W. Deming, and D. Barber (2013), Ikaite crystal distribution in winter sea ice and implications for CO_2 system dynamics. *Cryosph. 7*, 707–718.
Sarmiento, J. L., and N. Gruber (2006), *Ocean Biogeochemical Dynamics*, Princeton Univ. Press, Princeton, N. J.
Schmittner, A., N. Gruber, A. C. Mix, R. M. Key, A. Tagliabue, and T. K. Westberry (2013), Biology and air–sea gas exchange controls on the distribution of carbon isotope ratios (δ^{13}C) in the ocean, *Biogeosciences*, *10*(9), 5793–5816, doi:10.5194/bg-10-5793-2013.
Semiletov, I. P., I. I. Pipko, I. Repina, and N. E. Shakhova (2007), Carbonate chemistry dynamics and carbon dioxide fluxes across the atmosphere-ice-water interfaces in the Arctic Ocean: Pacific sector of the Arctic, *J. Mar. Syst.*, *66*, 204–226.
Shimada, K. (2005), Halocline structure in the Canada Basin of the Arctic Ocean, *Geophys. Res. Lett.*, *32*, L03605, doi:10.1029/2004GL021358.
Shimada, K., E. C. Carmack, K. Hatakeyama, and T. Takizawa (2001), Varieties of shallow temperature maximum waters in the western Canadian Basin of the Arctic Ocean, *Geophys. Res. Lett.*, *28*(18), 3441–3444.
Tanaka, T., Y. W. Watanabe, S. Watanabe, S. Noriki, N. Tsurushima, and Y. Nojiri (2003), Oceanic Suess effect of δ^{13}C in subpolar region: The North Pacific, *Geophys. Res. Lett.*, *30*(22), 2159, doi:10.1029/2003GL018503.
Thingstad, T. F., et al. (2008), Counterintutive carbon-to-nutrient coupling in an Arctic pelagic ecosystem, *Nature*, *455*, 388–390, doi:10.1038/nature07235.
Walsh, J. J., et al. (1989), Carbon and nitrogen cycling within the Berning/Chukchi Seas: Source regions for organic matter effecting AOU demands of the Arctic Ocean, *Prog. Oceanogr.*, *22*, 277–359.
Weingartner, T., D. J. Cavalieri, K. Aagaard, and Y. Sasaki (1998), Circulation, dense water formation, and outflow on shelf, *J. Geophys. Res.*, *103*(C4), 7647–7661.
Weiss, R. (1970), The solubility of nitrogen, oxygen and argon in water and seawater, *Deep Sea Res.*, *17*(4), 721–735.
Winsor, P., and D. C. Chapman (2002), Distribution and interannual variability of dense water production from coastal polynyas on the Chukchi Shelf, *J. Geophys. Res.*, *107*(C7), doi:10.1029/2001JC000984.
Woodgate, R., and K. Aagaard (2005), Revising the Bering Strait freshwater flux into the Arctic Ocean, *Geophys. Res. Lett.*, *32*, L02602, doi:10.1029/2004GL021747.
Woodgate, R., K. Aagaard, J. H. Swift, K. K. Falkner, and W. M. J. Smethie (2005), Pacific ventilation of the Arctic Ocean's lower halocline by upwelling and diapycnal mixing over the continental margin, *Geophys. Res. Lett.*, *32*, L18609, doi:10.1029/2005GL023999.
Yamamoto-Kawai, M., E. C. Carmack, and F. A. McLaughlin (2006), Nitrogen balance and Arctic throughflow, *Nature*, *443*, 43, doi:10.1038/443043a.
Yamamoto-Kawai, M., F. A. McLaughlin, E. C. Carmack, S. Nishino, and K. Shimada (2008), Freshwater budget of the Canada Basin, Arctic Ocean, from salinity, δ^{18}O, and nutrients, *J. Geophys. Res.*, *113*, C01007, doi:10.1029/2006JC003858.
Yamamoto-Kawai, M., F. A. McLaughlin, E. C. Carmack, S. Nishino, K. Shimada, and N. Kurita (2009), Surface freshening of the Canada Basin, 2003–2007: River runoff versus sea ice meltwater, *J. Geophys. Res.*, *114*, C00A05, doi:10.1029/2008JC005000.
Yamamoto-Kawai, M., F. A. McLaughlin, and E. C. Carmack (2011), Effects of ocean acidification, warming and melting of sea ice on aragonite saturation of the Canada Basin surface water, *Geophys. Res. Lett.*, *38*, L03601, doi:10.1029/2010GL045501.
Yamamoto-Kawai, M., N. Tanaka, and S. Pivovarov (2005), Freshwater and brine behaviors in the Arctic Ocean deduced from historical data of δ^{18}O and alkalinity (1929–2002 A.D.), *J. Geophys. Res.*, *110*, C10003.
Zhang, J., P. D. Quay, and D. Wilbur (1995), Carbon isotope fractionation during gas-water exchange and dissolution of CO_2, *Geochim. Cosmochim. Acta*, *59*(1), 107–114.